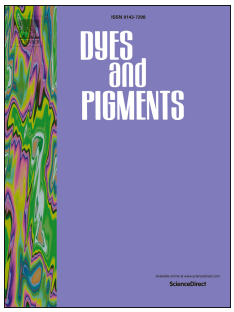

Novel triphenylamine polyamides bearing carbazole and aniline substituents for multi-colored electrochromic applications

Yu Liu, Tingjun Liu, Lifei Pang, Jinyu Guo, Jiuyang Wang, Duo Qi, Wenze Li, Kunzhi Shen

PII: S0143-7208(19)32148-5

DOI: https://doi.org/10.1016/j.dyepig.2019.107995

Reference: DYPI 107995

To appear in: *Dyes and Pigments*

Received Date: 23 September 2019

Revised Date: 23 October 2019

Accepted Date: 23 October 2019

Please cite this article as: Liu Y, Liu T, Pang L, Guo J, Wang J, Qi D, Li W, Shen K, Novel triphenylamine polyamides bearing carbazole and aniline substituents for multi-colored electrochromic applications, *Dyes and Pigments* (2019), doi: https://doi.org/10.1016/j.dyepig.2019.107995.

Novel triphenylamine polyamides bearing carbazole and aniline substituents for multi -colored electrochromic applications

Yu Liu[a], Tingjun Liu[a], Lifei Pang[a], Jinyu Guo[a], Jiuyang Wang[a], Duo Qi[a], Wenze Li[a,*], Kunzhi Shen[b]

[a] College of Applied Chemistry, Shenyang University of Chemical Technology, Shenyang, 110142, China

[b] Shenyang Photosensitive Chemical Research Institute Co., Ltd, Shenyang, 110141, China

Abstract:

A novel carbazolyl-derived diamine containing triphenylamine, 4,4'-bis[(4-aminophenyl)amino]-4''-carbazolyltriphenylamine (VI), was prepared via the reduction of 4,4'-bis[(4-nitrophenyl)amino]-4''-carbazolyltriphenylamine. A series of novel polyamides (PAs, individually denoted as VIIIA-VIIID) bearing carbazole-substituted triphenylamine units were subsequently prepared by direct polymerization of a novel diamine monomer (VI) and various aromatic diacids (VIIA-VIID). Cyclic voltammetry of the PAs cast onto an indium tin oxide (ITO) coated glass substrates revealed two reversible redox couples at 0.36-0.90 and 1.46-1.70 V under anodic scanning. Characterization of PA-VIIID showed that the resulting radical cations had excellent electrochromic properties, with their color changing from light yellow to green upon oxidation, and finally to dark blue in their fully oxidized form. Further, the optical contrast at 424 nm was 58.7%, while that at 820 nm was 74.2%. The coloring time at the specified wavelength of 424 nm was 3.4 s (during the oxidation process), the fading time was 3.9 s (during the reduction process), the coloring time at the specified wavelength of 820 nm was 3.9 s (during the oxidation process), and the fading time was 3.9 s (during the reduction process). In addition, the anodic coloring of the PA-VIIID showed a high coloring efficiency (CE = 203 cm^2/C), and the long-term redox reversibility was measured according to the difference in the percentage of transmittance exhibited by PA-VIIID between 0.00 and 1.70 V.

KEYWORDS: polyamide; electrochromism; aniline; triphenylamine

1. Introduction

Electrochromism refers to a phenomenon in which a material undergoes a reversible, stable color change under the action of an applied electric field, and a material exhibiting electrochromic properties is known as an electrochromic material [1-5]. Electrochromic materials are most commonly used in high-tech products such as displays, smart windows, optical glass and mirrors [6-14]. In the research and development of electrochromic materials, aniline, triphenylamine (TPA), and carbazole are often introduced as fundamental structures [15], in which aniline is used as an electrochromic element, and various electrochromic polymers can be prepared via covalent bond linking. Aniline has the advantages of high conductivity, good environmental stability and reversible redox behavior [16], In addition, it has good

electrochromic properties in hydrochloric acid, and thus it has been an important component of electrochromic materials [17-20]. Electrochromic materials containing the organic electroactive compound TPA and its derivatives have good thermodynamic, electrochemical, and optical properties, while the central nitrogen atom can be readily oxidized and TPA triphenylamine units have the ability to form free radical cations to transport positive charges. TPA also has a certain redox activity as well as strong electron donor and hole transport properties, and is thus considered to be an excellent electrochromic material [21-25]. Meanwhile, carbazole is another well-known high-performance electrochromic unit and hole transport material due to its large π-conjugated rigid planar structure and its electron-rich nitrogen-containing heterocyclic ring [26-29]. It is readily functionalized (at the 3,6-, 2,7- or *N*-positions) and can then be covalently attached to polymer systems, acting as a block in the backbone chain or as a substituent in the side-chains, thus providing a novel polyamide with enhanced electrochromic properties [30]. Therefore, polymers having these functional group properties and structures are often used for the preparation of electrochromic materials, and have considerable practical and commercial value [31].

In recent years, electrochromic materials based on TPA structural frameworks and incorporating other functional groups have been reported as active sites, and since they have certain electrochemical properties as well as a desirable oxidation-reduction potential, they are suitable for use as various electrochromic materials [32-34]. For example, Zheng et al. [35] designed and synthesized an electroactive polyamide incorporating alkyl chains in the backbone chain and a triarylamine unit as a functional group. The introduced alkyl group provided flexibility to the polyamide. The main polyamide absorption peak appeareds near λ_{max} = 283-296 nm, and this polyamide exhibited a photoluminescence PL peak at 363-404 nm in NMP, which could change from a nearly colorless neutral form to a green species upon oxidation, and subsequently a dark green oxidized form was formed once the polymer was fully oxidized. In addition, the polymer also had a low threshold voltage E_{SET} of -1.6 V and a E_{RESET} value of 4.2 V, which demonstrated the excellent electrochromic properties of this polymer. Meanwhile, Pan et al. [36] synthesized two novel electrochromic polyamides with hydroxyl functional groups. Since the hydroxyl skeleton can serve as an active site in sol-gel reaction, it can be effectively released during the redox process. The electrons are converted via strong electron absorption by covalent bonding, thereby greatly promoting the coloring and bleaching process. The TPPA-PATi5/HV device showed coloring behavior at 1.05 V over a period of 22.5 s, with a bleaching voltage of 1.1 V and a switching time of 5.2 s; while the device based on TPPA-PATi10/HV showed coloring behavior at 1.0 V over a period of 18.0 s, while the bleaching voltage was 1.05 V and the switching time was 5.0 s; and lastly the device based on TPPAPATi20/HV displayed coloring bahavior at 1.0 V and 17 s, with a bleaching voltage of 1.05 V and a switching time of 5.0 s. These results show that they have exhibit excellent electrochromic properties in terms of their switching and response times. Cheng et al. [37] reported novel electrochromic and aggregation-enhanced emission AEE active triphenylamine TPA-based polyamides that were prepared with 4-cyanotriphenylamine TPA-CN, 4-methoxytriphenylamine TPA-OMe, cyclohexane CH and tetraphenylethene TPE moieties via condensation polymerization. The introduction of an electron-donating methoxy substituent into the TPA moiety was found to effectively inhibit oxidation and enhance the corresponding electrochemical conversion, and a high-performance electrochromic device based on TPA-CN-CH/HV was used as a photoluminescence membrane. Electrochromic

devices based on TPA-CN-CH/HV (with a high photoluminescence quantum yield of 46%) as the active layer revealed the highest contrast ratio I_{off}/I_{on} of 105. The HV-containing TPA-OMe-TPE/HV-based electrochromic device exhibits a minimum response time of less than 4.9 s, which explains why the aromatic polyamide triggers a low voltage, has a short response time, and exhibits excellent electrochromic properties.

Our research team has reported various electrochromic polymer-based materials, such as novel polyamide-imides (PAIs) containing carbazole-substituted TPA units, there are two reversible redox couples at 1.05-1.08 and 1.38-1.46V by anode scanning, which shows that the resulting free radical cations have excellent electrochromic properties. During an anodic sweep, the color of this material changes from the original pale yellow that was observed in the neutral form to green, and then to the dark blue in the fully oxidized form. In addition, the anodic coloring of PAI showed a high coloring efficiency (CE = 205 cm^2/C), high contrast of light transmittance (ΔT = 80% at 776 nm) and robust redox reversibility [38]. In addition, the novel polyesterimide (PEI) bearing TPA and carbazole substituents, as well as the PEI-based films have shown excellent optical transparencies of 71-83%, 91-95%, and 94-97% at 450, 550, and 800 nm, respectively. Cyclic voltammetry measurements have revealed that the films exhibit two reversible redox couples at 1.06-1.12 and 1.44-1.79 V under an anodic sweep, with radical cations exhibiting outstanding stability. Additionally, anodic coloring (CE = 191 cm^2/C) tests have shown that these materials have a high optical contrast ratio and coloring efficiency [39]. In the past reports, the color-changing groups that were introduced to our designed electrochromic polymers have included both carbazole and TPA structures, and we are not aware of any reports in which three electrochromic groups are simultaneously introduced into such structures.

In order to enhance the electrochromic properties of the PAs, this experiment used a design in which three color-changing groups: aniline, TPA and carbazole were simultaneously introduced into a new diamine monomer structure. The obtained PAs are expected to possess a combination of desirable features, including high solubility, excellent thermostability, robust cycling stability, high color contrast and rapid switching speed. These findings demonstrate the promising potential of the PAs as electrochromic materials with a broad range of potential applications.

2. Measurements

^{1}H and ^{13}C nuclear magnetic resonance (NMR) spectra were recorded using a Bruker Ascend 500 MHz spectrometer and tetramethylsilane was employed as a reference. Cyclic voltammetry measurements were performed using a three-electrode cell. ITO (with PA film areas of -0.8 cm × 2.5 cm) was used as a working electrode, platinum wire was employed as an auxiliary electrode, and Ag/AgCl (using a saturated KCl solution) was used as a self-made reference electrode to record all of the battery potentials. The voltammogram exhibited an increase in the potential that was arranged to the left and the anodic current was directed downward. Absorption spectra were recorded using a Shimadzu UV 3101-PC spectrophotometer. Fourier-transform infrared spectroscopy (FT-IR) was performed using a Nicolet Impact 410 Fourier transform infrared spectrometer. Thermogravimetric measurements were carried out using a thermogravimetric analyzer (TGA) at a heating rate of 10 °C/min in a nitrogen atmosphere, and the PA samples were each loaded into an open

aluminum pan equipped with a METTLER TGA/DSC 1 Synchronous Thermal Analyzer. Photoluminescence spectra were measured using a Jasco FP-6300 fluorescence spectrophotometer. Characterization of the PAs was performed on Si/SiO_2 films via atomic force microscopy (AFM, Bruker MultiMode 8, tapping mode). Elemental analysis was performed using a MOD-1106 elemental analyzer system. Viscosity measurements were conducted using an Ubbelohde viscometer.

3. Experimental

3.1. Materials

Carbazole (99%, TCI), palladium (containing 10 wt% charcoal, denoted as Pd/C, Aldrich), *p*-fluoronitrobenzene (98%, TCI), 4,4'-dicarboxybiphenyl sulfone (99%, TCI), 4,4'-dicarboxydiphenyl ether (98%, TCI), 2,2-bis(4-carboxyphenyl)hexafluoropropane (98%, TCI), terephthalic acid (99%, TCI), anhydrous calcium chloride (99%, Aldrich), anhydrous potassium carbonate (K_2CO_3, 99%, Aldrich), tetrabutylammonium perchlorate (TBAP, 98%, Aldrich), *N*-methyl-2-pyrrolidone (NMP, 99.5%, Aldrich), hydrazine hydrate (85%, Aldrich), ethanol (EtOH, 99.7%, Aldrich), pyridine (Py, 97%, Aldrich), triethylamine (99.5%, Aldrich), *N*,*N*-dimethylformamide (DMF, 99.5%, Aldrich), acetic anhydride (AA, 98%, Aldrich), hydrochloric acid (HCl, 98%, Aldrich), *N*,*N*-dimethylacetamide (DMAc, 99%, Aldrich), tetrahydrofuran (THF, 99%, Aldrich), triphenyl phosphate (TPP, 97%, Aldrich), acetonitrile (99%, Aldrich), and dimethyl sulfoxide (DMSO-d_6, 99.5%, Aldrich) were used as received without further purification.

3.2. Monomer synthesis

3.2.1. Synthesis of *N*-(4-nitrophenyl)carbazole (I)

Carbazole (16.7 g, 100 mmol), *p*-fluoronitrobenzene(15.5 g, 100 mmol) and potassium carbonate(15.1 g, 100 mmol) were successively added into a 250 mL round-bottom flask that was equipped with a stir bar and dissolved in DMF (120 mL). Under nitrogen protection, the reaction system was stirred for 5-10 min at room temperature, then thoroughly mixed and, heated to 150-160 °C to reach a reflux state. This reflux was maintained, for 24 h. After the reaction was complete, the mixture was cooled to room temperature, and slowly poured into ice water. This mixture was then slowly stired to obtain a light yellow flocculent precipitate. After the ice had completely melted, this mixture was filtered. The filter cake was dried via suction filtration, washed repeatedly with water (7-8 times), washed repeatedly with distilled water (3-4 times), and finally washed 3-4 times with anhydrous methanol. It was then dried in a vacuum oven at 60 °C for 12 h. The crude product *N*-(4-nitrophenyl)carbazole was thus obtained. The weight of this dried product was 28.0 g, the theoretical yield was 28.8 g, and the percentage yield was 97.2%.

Monomer (I), light yellow powder, the yield was 97.2%. T_m: 208-210 °C, FT-IR (KBr) cm^{-1}: 1580, 1312 (NO_2 stretch). ^1H NMR (DMSO-d_6, 500 MHz, δ, ppm): 8.50 (2H, d, J = 7.5 Hz), 8.27 (2H, d, J = 7.7 Hz), 7.97 (2H, d, J = 8.1 Hz), 7.56 (2H, d, J = 8.2 Hz), 7.48 (2H, t, J = 7.9 Hz), 7.35 (2H, t, J = 7.3 Hz). Found: C, 75.0; H, 4.3; N, 9.9%; molecular formula $C_{18}H_{12}N_2O_2$ requires C, 75.0; H, 4.2; N, 9.7%.

3.2.2. Synthesis of *N*-(4-aminophenyl)carbazole (II)

The dried nitro compound *N*-(4-nitrophenyl)carbazole (monomer I in Scheme 1, 8.6 g, 30 mmol), along with the palladium carbon hydrogenation catalyst (Pd/C, 0.7 g, 10 wt%), and hydrazine hydrate (24 mL) were carefully weighed or measured. Monomer I and the Pd/C hydrogenation catalyst were then sequentially added to a 250 mL three-necked flask that was equipped with a stir bar. After the addition of ethanol (50 mL), this mixture was stirred at room temperature for 5-10 minutes until the reaction system was uniformly mixed, and it was then heated to 60 °C. After the temperature had become stable, the hydrazine hydrate was added dropwise to the reaction system through a constant pressure funnel at a controlled rate of 4-5 s per drop, so that the hydrazine hydrate was completely added within 2 h, and the reaction proceeded at a constant temperature for 12 h. After the reaction reached completion, Pd/C was removed via filtration through a sand core funnel. The filtrate was collected and the ethanol and hydrazine hydrate were distilled off via rotary evaporation, and the residual liquid was taken up in water to give a white precipitate. After washing with distilled water for 4-5 times, this precipitate was dried in a vacuum oven at 60 °C for 12 h. The crude product *N*-(4-aminophenyl)carbazole was thus obtained with a dried weight of 6.2 g, a theoretical yield of 7.7 g, and a percentage yield of 79.8%. The crude product was recrystallized from absolute ethanol under a nitrogen atmosphere at 85 °C, and the resultant crystals were dried in a vacuum oven at 60 °C for 12 h, thus yielding 5.2 g of the purified product as brown crystals.

Monomer (II), brown crystals, the yield was 79.8%. T_m: 105-107 °C, FT-IR (KBr) cm^{-1}: 3460, 3379 (NH_2 stretch). ^1H NMR (DMSO-d_6, 500 MHz, δ, ppm): 8.19 (2H, d, J = 7.7 Hz), 7.39 (2H, d, J = 8.3 Hz), 7.24 (4H, t, J = 7.5 Hz), 7.18 (2H, d, J = 7.2 Hz), 6.80 (2H, d, J = 7.0 Hz), 5.43 (2H, s). Found: C, 83.3; H, 5.5; N, 5.7%; molecular formula $C_{18}H_{14}N_2$ requires C, 83.7; H, 5.5; N, 5.8%.

3.2.3. Synthesis of 4,4'-dinitro-4''-*N*-carbazolyltriphenylamine (III)

Monomer II (9.0 g, 35 mmol), *p*-fluoronitrobenzene(10.8 g, 77 mmol) and potassium carbonate (10.6 g, 77 mmol) were placed in a 250 mL round-bottom flask that was equipped with a stir bar and then dissolved in DMF (80 mL). Under nitrogen protection, this reaction mixture was stirred for 5-10 min at room temperature until it was thoroughly mixed, and heated to 150-160 °C to reach a reflux state. This reflux was maintained at this temperature for 24 h. After the reaction was finished, the solution was cooled to room temperature, and it was then slowly poured into ice water. This mixture was slowly stirred to obtain a brownish yellow flocculent precipitate. After the ice had completely melted, this mixture was filtered. The filter cake was then dried via suction filtration, washed repeatedly with water for 7-8 times, washed repeatedly with distilled water for 3-4 times, and finally washed 3-4 times with anhydrous methanol. It was dried in a vacuum oven at 60 °C for 12 h. The crude product 4,4'-dinitro-4''-*N*-carbazolyl triphenylamine was thus obtained at a dried weight of 11.6 g, a theoretical yield of 17.5 g, and a percentage yield of 66.4%.

Monomer (III), brownish yellow powder, the yield was 66.4%. T_m: 281-283 °C, FT-IR (KBr) cm^{-1}: 1578, 1311 (NO_2 stretch). ^1H NMR (DMSO-d_6, 500 MHz, δ, ppm): 8.25 (6H, d, J = 8.1 Hz), 7.75 (2H, d, J = 8.2 Hz), 7.53 (2H, d, J = 7.4 Hz), 7.48 (4H, d, J = 7.6 Hz), 7.36 (4H, d, J = 9.1 Hz), 7.31 (2H, t, J = 6.8 Hz). Found: C, 72.0; H, 4.0; N, 11.3%; molecular formula $C_{30}H_{20}N_4O_4$ requires C, 72.0; H, 4.0; N, 11.2%.

3.2.4. Synthesis of 4,4'-diamino-4''-*N*-carbazolyltriphenylamine (IV)

The dinitro compound 4,4'-dinitro-4''-*N*-carbazolyltriphenylamine (monomer III in Scheme 1, 8.5 g, 17 mmol), Pd/C (0.4 g, 10 wt%), and hydrazine hydrate (13.6 mL) were accurately weighed or measured. Subsequently, monomer III and the Pd/C hydrogenation catalyst were sequentially added to a 250 mL three-necked round-bottom flask that was equipped with a stir bar. Ethanol (130 mL) was subsequently added and this mixture was stirred at room temperature for 5-10 min or until the reaction system was uniformly mixed, and it was then heated to 60 °C. After the temperature had become stable, the hydrazine hydrate was added dropwise to the reaction system through a constant pressure funnel at an addition rate of 4-5 s/drop, so that the hydrazine hydrate was completely added within 2 h, and the reaction was allowed to proceed at a constant temperature for 12 h. After the reaction was completed, the Pd/C catalyst was removed by filtration through a sand core funnel. The filtrate was then collected and ethanol and hydrazine hydrate were distilled off via rotary evaporation, and the residual liquid was mixed with water a dark red precipitate. After the precipitate had been washing with water 4-5 times and then with distilled water for 4-5 times, it was dried in a vacuum oven at 60 °C for 12 h. The crude product 4,4'-diamino-4''-*N*-carbazolyltriphenylamine was thus obtained at a dried weight of 7.0 g, a theoretical yield of 7.5 g, and a percentage yield of 93.6%. The crude product was recrystallized from absolute ethanol under a nitrogen atmosphere at 85 °C, and the resultant crystals were dried in a vacuum oven at 60 °C for 12 h, thus yielding 4.6 g of the purified diamine product in the form of dark crystals.

Monomer (IV), dark crystal, the yield was 93.6%. T_m: 110-112 °C, FT-IR (KBr) cm^{-1}: 3467, 3455 (NH_2 stretch). ^{1}H NMR (DMSO-d_6, 500 MHz, δ, ppm): 8.19 (2H, d, J = 7.7 Hz), 7.39 (2H, t, J = 7.6 Hz), 7.29 (2H, d, J = 7.3 Hz), 7.23 (2H, d, J = 7.2 Hz), 6.69 (2H, d, J = 7.1 Hz), 6.76 (2H, d, J = 7.0 Hz), 6.58 (8H, d, J = 7.4 Hz). 5.05 (4H, s). ^{13}C NMR (DMSO-d_6, 126 MHz, δ, ppm): 149.68, 146.67, 141.18, 135.80, 128.38, 127.74, 126.47, 126.42, 122.77, 120.83, 119.97, 116.81, 115.40, 110.14. Found: C, 81.7; H, 5.4; N, 12.6%; molecular formula $C_{30}H_{24}N_4$ requires C, 81.8; H, 5.5; N, 12.7%.

3.2.5. Synthesis of 4,4'-bis[(4-nitrophenyl)amino]-4''-carbazolyltriphenylamine (V)

A diamino compound (monomer IV in Scheme 1, 7.0 g, 16 mmol), *p*-fluoronitrobenzene (8.3 g, 59 mmol) and triethylamine (7.3 g) were sequentially added to a 100 mL round-bottom flask that was equipped with a stir bar and then dissolved in DMSO (40 mL). Under nitrogen protection, the reaction system was stirred for 5-10 min at room temperature, and then heated to reflux at 120-130 °C. The mixture was refluxed at this temperature for 72 h. After the reaction reached completion, it was cooled to room temperature, and the reaction solution was slowly poured into ice water. This mixture was slowly stirred to obtain a blood red flocculent precipitate. After the ice had completely melted, it was filtered, and the filter cake was collected via suction filtration. This precipitate was washed repeatedly (4-5 times) with water, then repeatedly washed (3-4 times) with distilled water, and finally washed with anhydrous methanol (3-4 times). It was subsequently dried in a vacuum oven at 60 °C for 12 h to yield the crude product 4,4'-bis[(4-nitrophenyl)amino]-4''-carbazolyltriphenylamine at a dried weight of 8.7 g, a theoretical yield of 10.9 g, and a percentage yield of 80.0%.

Monomer (V), reddish brown powder, the yield was 80.0%. T_m: 198-202 °C, FT-IR (KBr) cm^{-1}: 1593, 1323 (NO_2 stretch). ^1H NMR (DMSO-d_6, 500 MHZ, δ, ppm): 9.32 (2H, s), 8.25 (2H, d, J = 7.8 Hz), 8.11 (4H, d, J = 9.0 Hz), 7.51 (4H, d, J = 8.5 Hz), 7.42 (8H, m), 7.25 (6H, m), 7.08 (4H, d, J = 7.4 Hz). ^{13}C NMR (DMSO-d_6, 126 MHz, δ, ppm): 151.29, 147.12, 142.70, 140.81, 138.17, 136.40, 130.35, 128.28, 126.69, 126.35, 122.95, 122.81, 120.96, 120.30, 113.72, 110.16. Found: C, 73.9; H, 4.4; N, 12.3%; molecular formula $C_{42}H_{30}N_6O_4$ requires C, 73.9; H, 4.4; N, 12.3%.

3.2.6. Synthesis of 4,4'-bis[(4-aminophenyl)amino]-4''-carbazolyltriphenylamine (VI)

The dried dinitro compound 4,4'-bis[(4-nitrophenyl)amino]-4''-carbazolyltriphenylamine (monomer V in Scheme 1, 2.1 g, 3.1 mmol), Pd/C catalyst (0.1 g, 10 wt%), and hydrazine hydrate (5 mL) were carefully weighed or measured. Monomer V and the Pd/C hydrogenation catalyst were sequentially added to a 100 mL three-necked round-bottom flask that was equipped with a stir bar. DMF (30 mL) was then added to this flask and the mixture was stirred at room temperature for 5-10 min or until the reaction system was uniformly mixed, and it was subsequently heated to 60 °C. After the temperature had become stable, the hydrazine hydrate was added dropwise to the reaction system through a constant pressure funnel at a rate of 4-5 s/drop over a period of 2 h, and this mixture was allowed to react at a constant temperature for 72 h. After this reaction reached completion, the Pd/C catalyst was removed via filtration through a sand core funnel. The filtrate was taken up in water to give a light gray precipitate, which was washed with water (4-5 times) and then with and then with distilled water (4-5 times) before it was dried in a vacuum oven at 60 °C for 12 h. The crude product 4,4'-bis[(4-aminophenyl)amino]-4''-carbazolyltriphenylamine was thus obtained at a dried weight of 1.6 g, the theoretical yield of 1.9 g, and a percentage yield of 84.5%.

Monomer (VI), gray powder, the yield was 84.5%. T_m: 120-122 °C, FT-IR (KBr) cm^{-1}: 3439, 3368 (NH_2 stretch). ^1H NMR (DMSO-d_6, 500 MHz, δ, ppm): 8.19 (2H, d, J = 7.8 Hz),7.49 (2H, s), 7.39 (2H, t, J = 7.6 Hz), 7.27 (6H, m), 7.04 (2H, d, J = 8.6 Hz), 6.84 (12H, m), 6.55 (4H, d, J = 8.4 Hz), 4.74 (4H, s). ^{13}C NMR (DMSO-d_6, 126 MHz, δ, ppm): 149.17, 144.49, 144.26, 141.18, 137.04, 132.30, 128.05, 127.80, 127.17, 136.37, 122.95, 122.83, 120.82, 119.95, 117.90, 115.33, 110.03. Found: C, 81.1; H, 5.5; N, 13.5%; molecular formula $C_{42}H_{34}N_6$ requires C, 81.0; H, 5.5, N, 13.5%.

3.3. Polymer synthesis

A series of four PAs were prepared via polycondensation reactions using both diamine and diacid monomers. The diamine monomer was 4,4'-bis[(4-aminophenyl)amino]-4''-carbazolyltriphenylamine (VI in Schemes 1 and 2), while the diacid monomers included 4,4'-dicarboxybiphenyl sulfone (VIIA), 4,4'-dicarboxydiphenyl ether (VIIB), 2,2-bis(4-carboxyphenyl)hexafluoropropane (VIIC), terephthalic acid (VIID). As shown in Scheme 2, the polymers are expressed as VIIIA-VIIID, wherein the letters A-D correspond to the respective monomer (VIIA-VIID). A typical polycondensation reaction was performed as follows: monomer VI (0.3114 g, 1 mmol) and terephthalic acid (0.0830 g, 1 mmol) were sequentially added to a 20 mL sample vial containing anhydrous calcium chloride (0.1 g), triphenyl phosphate (0.5 mL), Py (0.25 mL), and NMP (5 mL). This mixture was then heated

at 120 °C and stirred for 3 h, taken up in ethanol, and then left standing to obtain a green flocculated suspension. After washing for 3 times with ethanol, it was dried in a vacuum oven at 50 °C to obtain the desired PAs, which formed a tough fibrous precipitate. Other PAs were synthesized in a similar manner. The characterization of the target PAs is summarized as follows:

PA-VIIIA, green powder. FT-IR (KBr) cm^{-1}: 1662 (C = O stretching) 3315, 1595 (NH stretching). ^{1}H NMR (DMSO-d_6, 500 MHz, δ, ppm): 10.33 (2H, s), 8.11 (6H, m), 7.60 (8H, d, J = 8.9 Hz), 7.34 (2H, s), 7.26 (6H, m), 7.11 (12H, m), 6.75 (4H, t, J = 7.8 Hz). ^{13}C NMR (DMSO-d_6, 126 MHz, δ, ppm): 164.04, 149.17, 144.49, 144.26, 141.18, 139.00, 137.04, 136.37, 134.58, 132.30, 131.70, 130.72, 129.76, 129.46, 128.05, 127.80, 127.56, 127.17, 126.55, 122.95, 122.83, 120.82, 119.95, 118.05, 117.90, 115.33, 110.03. UV-Vis (NMP, nm): The absorption maxima of the solution and the membrane were observed at 330 and 328 nm, respectively. Fluorescence (NMP, nm): The excitation and emission maxima were observed at 317 and 447 nm, respectively. The Stokes shift was observed at 130 nm.

PA-VIIIB, black powder. FT-IR (KBr) cm^{-1}: 1662 (C = O stretching) 3305, 1597 (N-H stretching). ^{1}H NMR (DMSO-d_6, 500 MHz, δ, ppm): 10.14 (2H, d, J = 4.6 Hz), 8.19 (4H, m), 8.03 (4H, m), 7.65 (4H, d, J = 8.5 Hz), 7.50 (4H, m), 7.20 (6H, m), 7.11 (12H, t, J = 7.0 Hz), 7.03 (4H, d, J = 8.6 Hz). ^{13}C NMR (DMSO-d_6, 126 MHz, δ, ppm): 149.17, 144.49, 144.26, 141.18, 138.89, 137.04, 135.52, 136.37, 134.20, 133.37, 132.30, 130.97, 129.87, 128.05, 127.80, 127.17, 122.95, 122.83, 122.33, 120.80, 120.82, 120.15, 119.95, 118.53, 117.90, 115.33, 110.03. UV-Vis (NMP, nm): The absorption maxima of the solution and the membrane were observed at 340 and 330 nm, respectively. Fluorescence (NMP, nm): The excitation and emission maxima were observed at 395 and 503 nm, respectively. The Stokes shift was observed at 108 nm.

PA-VIIIC, dark green powder. FT-IR (KBr) cm^{-1}: 1666 (C = O stretching) 3302, 1600 (N-H stretching). ^{1}H NMR (DMSO-d_6, 500 MHz, δ, ppm): 10.28 (2H, s), 8.19 (4H, m), 8.01 (4H, m), 7.60 (4H, s), 7.46 (4H, m), 7.33 (2H, s), 7.24 (4H, m), 7.12 (12H, m), 6.74 (4H, t, J = 9.2 Hz). ^{13}C NMR (DMSO-d_6, 126 MHz, δ, ppm): 156.38, 152.23, 149.17, 144.49, 144.26, 141.18, 138.06, 137.04, 136.37, 132.30, 130.52, 130.01, 128.05, 127.80, 127.17, 126.68, 125.26, 124.21, 122.95, 122.83, 122.11, 121.24, 120.82, 120.00, 119.95, 117.90, 117.40, 115.98, 115.33, 110.03. UV-Vis (NMP, nm): The absorption maxima of the solution and the membrane were observed at 341 and 339 nm, respectively. Fluorescence (NMP, nm): The excitation and emission maxima were observed at 320 and 445 nm, respectively. The Stokes shift was observed at 125 nm.

PA-VIIID, yellow green powder. FT-IR (KBr) cm^{-1}: 1666 (C = O stretch) 3308, 1600 (N-H stretch). ^{1}H NMR (DMSO-d_6, 500 MHz, δ, ppm): 10.27 (2H, s), 8.21 (2H, s), 8.05 (4H, d, J = 7.9 Hz), 7.66 (2H, s), 7.33 (4H, m), 7.26 (6H, m), 7.14 (12H, m), 7.03 (4H, t, J = 7.2 Hz). ^{13}C NMR (DMSO-d_6, 126 MHz, δ, ppm): 168.62, 167.28, 164.68, 151.57, 149.17, 144.49, 144.26, 141.18, 137.97, 137.04, 136.37, 132.30, 129.75, 128.05, 127.80, 127.17, 122.95, 122.83, 120.82, 119.95, 117.90, 115.33, 110.03. UV-Vis (NMP, nm): The absorption maxima of the solution and the membrane were observed at 339 and 324 nm, respectively. Fluorescence (NMP, nm): The excitation and emission maxima were observed at 315 and 443 nm, respectively. The Stokes shift was observed at 128 nm.

4. Results and discussion

4.1. Monomer synthesis

The novel monomer VI incorporating carbazole and TPA groups was synthesized via the route outlined in Scheme 1. In this experiment, the *N*-(4-nitrophenyl)carbazole (monomer I) is synthesized by nucleophilic aromatic substitution reaction by carbazole and 4-fluoronitrobenzene. The subsequent hydrogenation reaction with hydrazine hydrate mediated by the Pd/C catalyst yielded the amino-bearing compound *N*-(4-aminophenyl)carbazole (monomer II). 4,4'-Dinitro-4"-*N*-carbazolyltriphenylamine (monomer III) was subsequently synthesized via the nucleophilic aromatic substitution reaction of monomer II with *p*-fluoronitrobenzene. The dinitro-bearing monomer III was then reduced via the Pd/C hydrogenation catalyst-mediated hydrogenation reaction with hydrazine hydrate to obtain the diamino compound, 4,4'-diamino-4"-*N*-carbazolyltriphenylamine (monomer IV). Subsequently, monomer IV was nucleophilic aromatic substitution reaction with *p*-fluoronitrobenzene to synthesize 4,4'-bis[(4-nitrophenyl)amino]-4"-carbazolyl triphenylamine (monomer V), which was then reduced in the presence of the Pd/C hydrogenation catalyst and hydrazine hydrate to obtain 4,4'-bis[(4aminophenyl)amino]-4"-carbazolyltriphenylamine (monomer VI).

The ^{1}H NMR spectrum of the monomer V along with the corresponding signal assignments is shown in Figure 1. The proton labeled as “c” corresponds to the -NH proton and appears at the highest chemical shift of 8.32 ppm and is evidently deshielded by the nitrogen atom. Meanwhile, the proton at the “m” position appears at a relatively low field of 8.24 ppm, due to the strong electron-withdrawing effect of the carbazolyl N. The proton at the “b” site is located at the highest field of 7.08 ppm, due to the electron donating effect of the -NH moiety on the benzene ring. As shown in the H-H correlation spectrum (COSY) of the monomer V (Figure 2), each proton assignment is given and is consistent with those shown in Figure 1. In this COSY spectrum, the bimodal correlation of 8.06/7.04 ppm, 8.24/7.28 ppm and 7.50/7.28 ppm can be easily assigned to protons “a”, “b”, “m”, “l”, “k” on the aniline and carbazolyl benzene rings. As shown in Figure 3, a ^{13}C NMR spectrum of monomer V was recorded in the DEPT Q mode, and thus all of the quaternary carbon peaks are oriented downward. The carbon at position “7” showed the highest chemical shift in this spectrum at 151.37 ppm, while the carbon at position “5” was the most highly shielded at 110.12 ppm.

As shown in the ^{1}H NMR spectrum of monomer VI (Figure 4), the proton at the “h” position resonated at 7.03 ppm due to the presence of the -NH group in the structure of this monomer VI structure. Meanwhile, the proton at the “a” position was relatively shielded and resonated at 4.73 ppm, due to the presence of the electron donating -NH_2 group. The proton at the “g” position exhibited a signal at the lowest field highest chemical shift of 8.18 ppm. The proton at the “i” position was at a higher field of 6.54 ppm, due to the electron donating effect of the -NH_2 group. As shown in the COSY spectrum of monomer VI (Figure 5), each proton assignment is provided and is consistent with the proposed molecular structure. In this COSY spectrum, the bimodal correlation pairs observed at 8.18/7.24, 6.84/6.54, and 7.32/6.87 ppm, can readily be assigned to the protons at the “g”, “d”, “I”, “b”, “k”, and “c” positions. As shown in Figure 6, a ^{13}C NMR spectrum of monomer VI was recorded in the DEPT Q mode, and all of the quaternary carbon peaks are oriented downwards. The carbon at

the “7” position shows the lowest field signal at 151.37 ppm, while that at the “5” position shows the hight field signal 110.12 ppm.

4.2. Polymer synthesis

A series of novel PAs (VIIIA-VIIID) was prepared via the polymerization of the diamine monomer VI with the diacid compounds VIIA-VIID, as shown in Scheme 2. During the polymerization, triphenyl phosphate (TPP) and pyridine (Py) were used as condensing agents, anhydrous calcium chloride was dehydrated, and *N*-methyl-2-pyrrolidone (NMP) was used as a solvent. Each polymerization reaction was conducted in a uniform manner, and they ultimately yielded a dark and moderately viscous PA solution. The PAs solution was slowly poured into a stirred ethanol solution and allowed to stand until the PA formed a precipitate consisting of a tough fiber-like floc structure.

The elemental analysis data is provided in Table 1, and it can be observed that the experimental values and the corresponding theoretical values are consistent with one another. The intrinsic viscosities of the intermediate PAs were evaluated in DMAc at 25 °C with the use of an Ubbelohde viscometer. All of the PAs exhibited intrinsic viscosities in the range of 0.50-0.75 dL/g, the weight average molecular weight (M_ws) is recorded between 36,000 and 52,000, and the number average molecular weight (M_ns) is recorded between 21,000 and 26,000, relative to polystyrene standards. The range of polydispersity index (PDI) is between 1.7 and 2.0. All PAs can provide a soft, yet tough film because the molecular weights of them were high enough, and the details regarding these experiments are summarized in Table 2.

The chemical structures of the PAs were also characterized via FT-IR spectroscopy. As shown in Figure 7, the FT-IR bands of these PAs appear in various positions, ranging from 1666 to 1662 cm^{-1} (C = O stretching), 3315 to 3302 cm^{-1} (amide bond-NH stretching) and 1600 to 1595 cm^{-1} (-NH stretching). These signals correspond to the amide groups residing in the backbones of these polymers.

A ^{1}H NMR spectrum of the polymer PA-VIIID along with the corresponding signal assignments is shown in Figure 8. The proton residing at the “12” position in PA-VIIID appeared at 10.26 ppm and corresponded to the amide proton in the backbone of this polymer. Meanwhile, the proton at the “9” position resonated at 8.05 ppm due to the presence of the characteristic -NH group. The proton occupying the “11” position exhibited a high field resonance of 7.03 ppm due to the presence of the -NHCO- group and the -NH group’s electron donating effect. The proton labeled as “13” on the adjacent benzene ring exhibited a lower field resonance of 8.21 ppm and the proton residing at the “14” position displayed a lower field resonance of 7.67 ppm, due to the strong electron-withdrawing effect of the carbonyl moiety in the amide group. The proton labelled as “1” in Figure 8 exhibited a lower field of resonance 8.09 ppm, due to the presence of the strong electron-withdrawing effect of the carbazolyl nitrogen. The protons at the other positions were consistent with those found in monomer VI, and thus the signals that were consistent with the formation of the -NHCO- bond indicated that the polymerization reaction had indeed proceeded to produce the target PAs.

4.3. Solubilities of the PAs

The solubilities of the PAs synthesized herein were measured in various organic solutions at a solution concentration of 1.0 wt%. As shown in Table 3, the synthesized PAs had good solubilities in various solvents, including NMP, DMAc, DMF and DMSO. It was apparent that PA-VIIIA and PA-VIIIC were more soluble than PA-VIIIB and PA-VIIID. The better solubility of PA-VIIIA can be attributed to the presence of the polar sulfone groups in its structure. Meanwhile, the better solubility of PA-VIIIC is due to the presence of large pendant structures such as hexafluoroisopropyl in its structure. Hexafluoroisopropyl is a large pendant group with high bond energy. Its introduction hinders intramolecular electron transfer and destroys the conjugated structure, which reduces the bulk density between molecules, which in turn increases the solubility of the polymer.

4.4. Film formation behavior

PA samples (1.0 g) were weighed and dissolved in 10 mL of NMP solution to obtain solutions of these polymers, and they were then uniformly applied onto glass substrates to yield films. As shown in Figure 9, the coating obtained from PA-VIIID exhibited a uniform distribution, clearly showing its ordered linear and stepped structure, and it can sample the target PAs chain in a three-dimensional space. The root mean square (RMS) surface roughness was 0.15 nm and the maximum roughness was ~1.9 nm.

4.5. Optical properties of the PAs

The absorption wavelengths of the electronic transition spectra of the PAs ranged from 200 to 800 nm and UV-Visible spectroscopy is mainly used for the analysis of compounds containing conjugated structures. In this study, the ultraviolet absorption spectra of the PAs that had been dissolved in NMP are shown in Figure 10. The differences in the absorption spectra indicate that the concentrations of the corresponding monomer solutions were different, the concentration at the higher position is larger, and the concentration at the lower position is small. The absorption maxima were observed in the range of 330-341 nm, and these wavelengths exhibited red-shifts as the length of the conjugated chain grew longer. The absorption peaks observed in Figure 10 are rather intense, indicating that the PAs contain multiple conjugated π bonds, which provides further evidence that the PAs were successfully synthesized.

The fluorescence (PL) quantum yield ($Ø_{unk}$) of PAs in NMP was recorded and a H_2SO_4 solution of 0.5 mol L^{-1} quinine sulfate was typically used as a standard ($Ø_{std}$ = 0.546). Figure 11 also shows the PL spectrum (concentration: 10^{-6} mol L^{-1}) of PAs recorded in NMP solution. We calculate the quantum yield of PAs via formula (1) [40,41]:

$$\emptyset_{unk} = \emptyset_{std} \left(\frac{I_{unk}}{I_{std}}\right)\left(\frac{A_{std}}{A_{unk}}\right)\left(\frac{\eta_{unk}}{\eta_{std}}\right)^2 \quad (1)$$

Among them, $Ø_{unk}$, $Ø_{std}$, I_{unk}, I_{std}, A_{unk}, A_{std}, η_{unk} and η_{std} respectively denote the fluorescence quantum yields of the sample and standard, the integral of the emission intensity, the absorbance of the excitation wavelength and the refractive index of the relevant solvent. In NMP solution, PAs showed the largest fluorescence excitation peak at 395 nm, and PAs showed the largest fluorescence emission peak at the most 503 nm. The fluorescence quantum yield of PA-VIIIA is 0.532%, the fluorescence

quantum yield of PA-VIIIB is 0.637%, the fluorescence quantum yield of PA-VIIIC is 0.832%, the fluorescence quantum yield of PA-VIIID is 0.134%. Due to the self-quenching effect of intramolecular charge transfer, the fluorescence quantum yield is less than 1%.

As shown in Figure 11, the fluorescence excitation peaks exhibited by the PAs in NMP solutions ranged from 315 to 395 nm. The minimum fluorescence excitation wavelength was exhibited by PA-VIIID at 315 nm, while the maximum fluorescence excitation wavelength was exhibited by PA-VIIIB at 395 nm. The fluorescence emission peaks exhibited by these polymers range from 443 to 503 nm. The minimum fluorescence emission wavelength was exhibited by PA-VIIID at 443 nm, while the maximum fluorescence emission wavelength was exhibited by PA-VIIIB at 503 nm.

4.6. Thermal properties of the PAs

The data describing the thermal behavior of the PAs are summarized in Table 2. These PAs have T_g values in the range of 303-320 °C, and they increase in the order of PA-VIIIC < PA-VIIIB < PA-VIIID < PA-VIIIA. The glass transition temperatures of the PAs observed in this study were higher than the literature values for related examples that we had previously prepared. [39] These differences can be attributed to the introduction of the aniline group in the structures of the PAs, including the -NH bond residing in the aniline structure, as well as the presence of the hydrogen bonds involving this moiety which increase the intermolecular interaction forces, thus resulting in an increase in the glass transition temperature. The PA-VIIIA sample had the highest T_g value at 320 °C, apparently due to the presence of a rigid group sulfone group in its structure. Conversely, the PA-VIIIC had the lowest T_g value at 301 °C, evidently due to the presence of the hexafluoroisopropyl groups.

According to Figure 12, the PAs undergo a 5% weight loss as the temperature is increased from 338 to 460 °C. The PAs also experienced a 10% weight loss with an increasing temperature over the range from 451 to 532 °C. PA-VIIIA and PA-VIIIC begin to lose weight at lower temperaturs than their counterparts, evidently due to the presence of the sulfone and hexafluoroisopropyl units in PA-VIIIA and PA-VIIIC, respectively. In contrast, PA-VIIIB and PA-VIIID are relatively stable. As shown in Table 2, the total temperature of the PAs is relatively low, evidently due to the poor heat resistance of the aniline groups. The carbonization residue (coke yield) of these PAs measured between them is 800 °C in a nitrogen atmosphere, usually greater than 60%.

4.7. Electrochemical properties

Cyclic voltammetry was performed using a three-electrode cell in which ITO glass served as the working electrode, platinum wire served as the counter electrode, and silver wire was employed as the reference electrode. An acetonitrile solution of 0.1 M tetrabutylammonium perchlorate (0.6838 g of tetrabutylammonium perchlorate, 20 mL of acetonitrile solution) was used as the electrolyte solution, and the CV mode of the electrochemical workstation was employed for the measurements that were conducted over a range of 0-2 V. The resultant cyclic voltammograms are shown in Figure 13.

The reference electrode was calibrated with PA-VIIID/ferrocene salt (Fe/Fe^+), as shown in Figure 13. The redox standard E (Fe/Fe^+) was 0.48 V based on the (Fe/Fe^+)

standard. The HOMO level was 4.80 eV relative to the zero vacuum level. The HOMO value thus obtained was calculated from the HOMO level via cyclic voltammetry and referenced to ferrocene (4.80 eV). Since the LUMO value cannot be directly derived from the graph, the initial absorption wavelength value λ_{onset} had to be obtained from the ultraviolet-visible absorption spectrum, and subsequently the LUMO value was obtained by the following formula.

$$E_g(eV) = 1240 / \lambda_{onset} \tag{2}$$

$$HOMO = E_{onset} + 4.80 - E_{(Fe/Fe^+)} \tag{3}$$

$$LUMO = HOMO - E_g(eV) \tag{4}$$

Taking the typical CV curve of PA-VIIID as an example, when the applied oxidation potential is 0 V, the PA-VIIID exists in a reduced state. After the oxidation potential is increased, the PA-VIIID exhibits a first oxidation state, and the color of the PA-VIIID film changes. The oxidation potential is constantly changing. The measurement shows that the corresponding oxidation peaks appear at 0.90 and 1.70 V, and the corresponding reduction peaks appear at 0.36 V and 1.46 V. The PA-VIIID film undergoes a reversible redox reaction in an electrolyte solution. It can be seen from Figure 13 that under the anodice scanning, PA-VIIID exhibits two reversible redox couples. The two half-wave potentials occur at 0.63 V and 1.58 V. The initial potential (E_{onset}) is 0.30 V. Meanwhile, the initial absorption wavelength value λ_{onset} is obtained from the ultraviolet-visible absorption spectrum. λ_{onset} = 417 nm, which is brought into the formula (2) to obtain an E_g value of 2.97 eV. The initial potential (E_{onset}) was 0.30 V, the E (Fe/Fe^+) value was 0.48 V, and the HOMO value was 4.62 eV obtained by introducing it into the formula (3); the LUMO value was 1.65 eV by substituting the above value into the formula (4). The HOMO value of the PA-VIIID is calculated by the formula to be 4.62 eV, while the LUMO value is 1.65 eV and the E_g value is 2.97 eV. As shown in Table 4, PA-VIIIA has a HOMO value of 4.82 eV, a LUMO value of 1.70 eV, and an E_g value of 3.12 eV. Meanwhile, PA-VIIIB has a HOMO value of 4.90 eV, a LUMO value of 1.77 eV, and an E_g value of 3.13 eV. Lastly, PA-VIIIC has a HOMO value of 4.63 eV, a LUMO value of 1.58 eV, and an E_g value of 3.05 eV.

4.8. Electrochromic properties

The electrochromic properties of the PA-VIIID film were tested and characterized by the use of an electrochemical workstation and via UV-Vis spectroscopy (UV-Vis-NIR), while the electrode preparation methods and solution conditions were similar to those used for the CV measurements. A typical representative electrochromic absorption spectrum of the PA-VIIID film in a 0.1 M tetrabutylammonium perchlorate acetonitrile solution is exemplified by the spectrum shown in Figure 14. When the applied voltage is increased from 0 to 1.80 V, the characteristic absorption peak of PA-VIIID at 331 nm gradually decreases, and the absorbance values of the peaks at 424 and 820 nm gradually increase. When the voltage is 0 V, the original UV is observed, PA-VIIID is in a neutral state, and the color of this polymer is light yellow. As the voltage increases, the strength of the characteristic absorption peak of PA-VIIID decreases gradually at 331 nm, and PA-VIIID exhibits a stronger absorption and exists in a semi-oxidized state. The oxidation

reaction that takes place results in a new absorption peak for PA-VIIID at 424 nm. Meanwhile, the color of PA-VIIID changes from light yellow to green. As the voltage increases again, PA-VIIID becomes completely oxidized, and the oxidation reaction that occurs causes PA-VIIID to show a new absorption peak at 820 nm, while the color changes from green to dark blue. When a reverse voltage is applied, PA-VIIID returns to its reduced state, thus demonstrating that this is a reversible redox process.

The nitrogen atoms located at the aniline and amide linkages could be oxidized to cationic radicals while an electric field applied, causing the electrochromism to occur. In addition, the resultant color faded due to the reduction of the cation as the molecule returned to its neutral state. When the electrokinetic amino group is converted into a strongly electron-withdrawing ammonium group salt, its conjugation degree is changed and therefor the colour has changed. At the end of the oxidation-reduction process, the color of PA-VIIID returns to that of its original molecular state, demonstrating that this polymer has electrochromic properties.

As shown in Figure 15, the color value of PA-VIIID in an acetonitrile solution containing 0.1 M tetrabutylammonium perchlorate varies with the applied voltage. When the applied voltage is 0 V (CIE 1931: X 0.39, Y 0.38), the color appears light yellow; when the voltage becomes 0.9 V (CIE 1931: X 0.35, Y 0.55), the color appears light green; when the voltage becomes 1.6 V (CIE 1931: X 0.28, Y 0.49), the color is light blue-green; and finally, when the voltage rises to 1.8 V (CIE 1931: X 0.16, Y 0.09) the color appears blue and does not change further.

A typical representative electrochromic absorption spectrum of the PA-VIIID film in a 1 M hydrochloric acid solution is shown in Figure 16. When the applied voltage is increased from 0 to 1.20 V, the characteristic absorption peak of the PA-VIIID film at 330 nm gradually decreases in strength, and the strengths of the characteristic absorption peaks at 418 and 1007 nm gradually increase. When the voltage is 0 V, the original UV curve, is observed. In this scenario PA-VIIID is in a neutral state and appears light yellow. As the voltage increases, the characteristic absorption peak of PA-VIIID gradually decreases in strength at 330 nm, and PA-VIIID exhibits a high absorption and exists in a semi-oxidized state. This oxidation reaction causes PA-VIIID to generate a new absorption peak at 418 nm, and its color changes from light yellow to light green. As the voltage rises again, PA-VIIID becomes completely oxidized. The oxidation reaction that occurs at this stage causes the PA-VIIID to show a new absorption peak at 1007 nm, and its color changes from light green to dark green.

As shown in Figure 17, the color value of a PA-VIIID film in a 1 M hydrochloric acid solution changes with the applied voltage. When the applied voltage is 0 V (CIE 1931: X 0.36, Y 0.41), the color of this film appears light yellow; when the voltage becomes 0.6V (CIE 1931: X 0.35, Y 0.46), the color becomes yellow-green; and finally, when the voltage rises to 1.2V (CIE 1931: X 0.31, Y 0.58) the color becomes dark green and does not change further.

By analyzing the change of transmittance at 424 and 820 nm with time, the electrochromic properties of the PA-VIIID film were investigated, and the voltage was continuously switched between 0 V in the neutral state and 1.70 V in the fully oxidized state. During this test, the UV-Vis-NIR method was used to determine the percent transmittance at a particular wavelength. The changes in the transmittance of

the PA-VIIID film during the first 200 cycles at 424 and 820 nm can be seen from Figure 18 and 19, along with the differences in the transmittance percentage between 0 V and 1.70 V. During these measurements, the optical contrast at 424 nm was 58.7%, and the optical contrast at 820 nm was 74.2%. The changes in the transmittance of the PA-VIIID film during one cycle at 424 and 820 nm can be seen from Figure 20 and 21, and each cycle was performed over a duration of 12 s. According to calculations, the coloring time of the PA-VIIID film at a specific wavelength of 424 nm at an oxidation voltage of 1.70 V was 3.4 s (during the oxidation process), and the fading time at a reduction voltage of 0 V was 3.9 seconds (during the reduction process). In addition, the coloring time of the PA-VIIID film at a specific wavelength of 820 nm at an oxidation voltage of 1.70 V was 3.9 s (during the oxidation process), and the fading time at a reduction voltage of 0 V was 3.9 seconds (during the reduction process). According to Figure 18 and 19, the PA-VIIID film still had good electrochemical and electrochromic reversibility after 200 cycles of scanning between 0.00 and 1.70 V.

The electrochromic coloration efficiency (*CE*) can be calculated via the following equation:

$$CE = \Delta OD/Q$$

where ΔOD denotes the optical absorbance change and Q (mC/cm^2) represents the injected/ejected charge during a redox step. Based on this equation, it was found that at 820 nm, the *CE* of the PA-VIIID was 203 cm^2/C.

5. Conclusion

A series of novel redox-active PAs (VIIIA-VIIID) bearing three electrochromic groups: aniline, TPA and carbazole structures, were successfully by the direct polycondensation of the diamine monomer 4,4'-bis[(4-aminophenyl)amino]-4"-carbazolyltriphenylamine (VI) with diacid compound (VIIA-VIID). The obtained PAs exhibited high solubility in organic solvents, robust redox reversibility, long-term cycling stability, high color contrast, and exhibited rapid switching speeds. In addition, the PAs exhibit electrochromic behavior in both organic electrolyte solvents and in hydrochloric acid. These findings demonstrate the promising potential of the PAs as electrochromic materials with a broad range of potential applications.

Acknowledgements

We are grateful to the China Postdoctoral Science Foundation (2018M630309), Liaoning Provincial Department of Education Fund (LQ2019004) and National Natural Science Foundation (51903164) for the financial support.

References

[1] P.M.S. Monk, R.J. Mortimer and D.R. Rosseinsky, Electrochromism and Electrochromic Devices, *Angew. Chem.*, 2010, 47, 6945-6946.

[2] B.C. Thompson, P. Schottland, K. Zong, J.R. Reynolds, In Situ Colorimetric Analysis of Electrochromic Polymers and Devices, *Chem. Mater.*, 2000, 12, 1563-1571.

[3] T. Niwa, O. Takai, All-solid-state reflectance-type electrochromic devices using iridium tin oxide film as counter electrode, *Thin Sol. Films*, 2010, 518, 5340-5344.

[4] M. Nishikawa, K. Nomoto, S. Kume, H. Nishihara, Reversible copper(II)/(I) electrochemical potential switching driven by visible light-induced coordinated ring rotation, *J. Am. Chem. Soc.*, 2012, 134, 10543-10553.

[5] X. Luo, K.E. Lauber, P.T. Mather, A thermally responsive, rigid, and reversible adhesive, *Polymer*, 2010, 51, 1169-1175.

[6] H.W. Heuer, R. Wehrmann, S. Kirchmeyer, Electrochromic Window Based on Conducting Poly(3,4-ethylenedioxythiophene)-Poly(styrene sulfonate), *Adv. Funct. Mater.*, 2010, 12, 89-94.

[7] R.J. Mortimer, L. Aubrey, D. Yer, R. John, Reynolds, Electrochromic organic and polymeric materials for display applications, *Displays*., 2006, 27, 2-18.

[8] G. Sonmez, Sonmez, B. Hayal, Polymeric electrochromics for data storage, *J. Mater. Chem.*, 2006, 16, 2473-2477.

[9] P. Andersson, R. Forchheimer, P. Tehrani, M. Berggren, Printable All-Organic Electrochromic Active-Matrix Displays, *Adv. Funct. Mater.*, 2010, 17, 3074-3082.

[10] R. Baetens, B.J. Petter Jelle, A. Gustavsen, Properties requirements and possibilities of smart windows for dynamic daylight and solar energy control in buildings: A state-of-the-art review, *Sol. Energy Mater. Sol. Cells*, 2010, 94, 87-105.

[11] P.R. Somani, S. Radhakrishnan, Electrochromic materials and devices: present and future, *Mater. Chem. Phys.*, 2003, 77, 117-133.

[12] F. Lin, D. Nordlund, T.C. Weng, R.G. Moore, D.T. Gillaspie, A.C. Dillon, R.M. Richards, C. Engtrakul, Hole doping in Al-containing nickel oxide materials to improve electrochromic performance, *ACS Appl. Mater. Interfaces*, 2013, 5, 301-309.

[13] M.A. Warwick, R. Binions, Advances in thermochromic vanadium dioxide films, *J. Mater. Chem. A*, 2014, 2, 3275-3292.

[14] Y.C. Nah, S.S. Kim, J.H. Park, H.J. Park, J. Jo, D.Y. Kim, Enhanced electrochromic absorption in Ag nanoparticle embedded conjugated polymer composite films, *Electrochem. Commun.*, 2007, 9, 1542-1546.

[15] J. Kim, S.H. K, J. Kim, I. Kim, Y. Jin, J.H. Kim, H.Y. Woo, K. Lee, H. Suh, Di-aryl substituted poly(cyclopenta[def]phenanthrene) derivatives containing carbazole and triphenylamine units in the main chain for organic light-emitting diodes, *Macromol. Res.*, 2011, 19, 589-598.

[16] P.R. Somani, S. Radhakrishnan, Electrochromic materials and devices: present and future, *Mater. Chem. Phys.*, 2003, 77, 117-133.

[17] J.Y. Wang, C.M. Yu, S. Chia, H. wang, K.C. Ho, L.C. Chen, Influence of coloring voltage on the optical performance and cycling stability of a polyaniline-indium hexacyanoferrate electrochromic system, *Sol. Energy Mater. Sol. Cells*,

2008, 92, 112-119.
[18] A Yağan, N.O. Pekmez, A. Yıldız, Corrosion inhibition by poly(*N*-ethylaniline) coatings of mild steel in aqueous acidic solutions, *Prog. Org. Coat.*, 2006, 57, 314-318.
[19] K.F. Khaled, N. Hackerman, Ortho-substituted anilines to inhibit copper corrosion in aerated 0.5 M hydrochloric acid, *Electrochim. Acta*, 2004, 49, 485-495.
[20] M. Grigoras, L. Vacareanu, T. Ivan, A.M. Catargiu, Photophysical properties of isoelectronic oligomers with vinylene, imine, azine and ethynylene spacers bearing triphenylamine and carbazole end-groups, *Dyes and Pigments*, 2013, 98, 71-81.
[21] K.L. Wang, Y.L. Liu, J.W. Lee, K.G. Neoh, Nonvolatile electrical switching and write-once read many-times memory effects in functional polyimides containing triphenylamine and 1, 3, 4-Oxadiazole moieties, *Macromolecules*, 2010, 43, 7159-7164.
[22] F. Arab, F.A. Sahraoui, K. Haddadi, L. Louail, Ab initio investigations of structural, elastic and electronic properties of $ZnSiP_2$: pressure effect computational, *Comput. Mater. Sci.*, 2012, 65, 520-527.
[23] A. Iwan, D. Sek, Polymers with triphenylamine units: photonic and electroactive materials, *Prog. Polym. Sci.*, 2011, 36, 1277-1325.
[24] M. Ouyang, Z.Y. Fu, X.J. Lu, H.L. Chen, B. Hu, X.F. Xia, C. Zhang, Enhanced film-forming and electrochromic properties by incorporating bithiophene into triphenylamine, *Acta Phys. Chim. Sin.*, 2005, 29, 996-1002.
[25] C.J. Chen, Y.C. Hu, G.S. Liou, Linkage and acceptor effects on diverse memory behavior of triphenylamine-based aromatic polymers, *Polym. Chem.*, 2013, 4, 4162-4171.
[26] M. Jean-Francois, L. Mario, A. Dominique, S. Alain, Polycarbazoles: 25 Years of Progress, *Macromol. Rapid Comm.*, 2005, 26, 761-778.
[27] Y.Y. Liu, W.M. Li, A.R. Hlil, Y.Z. Meng, A.S. Hay, Synthesis and properties of carbazole-containing copolymers from bis[3-(4-fluorobenzoyl)carbazole] methane, *J. Incl. Phenom. Macro.*, 2010, 47, 1051-1054.
[28] S.H. Hsiao, H.M. Wang, J.W. Lin, W.J. Guo, Y.R. Kung, C.M. Leu, T.M. Lee, Synthesis and electrochromic properties of polyamides having pendent carbazole groups, *Mater. Chem. Phys.*, 2013, 141, 665-673.
[29] H.M. Wang, S.H. Hsiao, Substituent effects on electrochemical and electrochromic properties of aromatic polyimides with 4-(carbazol-9-yl)triphenylamine moieties, *J. Polym. Sci.*, 2014, 52, 1172-1184.
[30] M. Leclerc, Najari, Ahmed, Beaupré, Serge, 2008 Macromolecular Science and Engineering Division Award Lecture-Conjugated polymers: From micro-electronics to genomics, *Can. J. Chem.*, 2009, 87, 1201-1208.
[31] S.H. Fu, M. Higuchi, Y. Akasaka, Y. Otsuka, D.G. Kurth, Preparation, characterization, and electrochromic properties of novel Co(II)-bis-2,2':6',2"-terpyridine metallo-supramolecular polymers, *Thin Sol. Films*, 2008, 516, 2469-2473.
[32] J.C. Lai, X.R. Lu, B.R. Lu, F. Liu, C.H. Li, X.Z. You, A new multicolored and near-infrared electrochromic material based on triphenylamine-containing poly (3,4-dithienylpyrrole), *Org. Electron.*, 2014, 15, 3735-3745.
[33] S.X. Xiong, S.S. Li, X.K. Zhang, R. Wang, R.L. Zhang, X.Q. Wang, B.H. Wu, M. Gong, J. Chu, Synthesis and Performance of Highly Stable Star-Shaped Polyaniline Electrochromic Materials with Triphenylamine Core, *J. Electron.*

Mater., 2018, 47, 1167-1175.

[34] Y.W. Chuang, H.J. Yen, J.H. Wu, G.S. Liou, Colorless Triphenylamine-Based Aliphatic Thermoset Epoxy for Multicolored and Near-Infrared Electrochromic Applications, *ACS Appl. Mater. Interfaces*, 2014, 6, 3594-3599.

[35] R.R. Zheng, X. Zhang, Z.P. Zhang, H.J. Niu, C. Wang, W. Wang, Preparation and multifunction of electrochromic polyamides containing flexible backbone chains with electrochemical, fluorescence and memory properties, *Appl. Surface Sci.*, 2019, 478, 906-915.

[36] B.C. Pan, W.H. Chen, T.M. Lee, G.S. Liou, Synthesis and characterization of novel electrochromic devices derived from redox-active polyamide-TiO_2 hybrids, *J. Mater. Chem. C*, 2018, 6, 12422-12428.

[37] S.W. Cheng, T. Han, T.Y. Huang, B.Z. Tang, G.S. Liou, High-performance electrofluorochromic devices based on aromatic polyamides with AIE-active tetraphenylethene and electro-active triphenylamine moieties, *Polym. Chem.*, 2018, 9, 4364-4373.

[38] Y. Liu, D.M. Chao, H.Y. Yao, New triphenylamine-based poly(amine-imide)s with carbazole-substituents for electrochromic applications, *Org. Electron.*, 2014, 15, 1422-1431.

[39] Y. Liu, L. Liu, B.Y. Ren, X.Y. Zhu, W.Y. Zhou, W.Z. Li, Novel low color poly(ester imides) with triphenylamine and carbazole substituents for electrochromic applications, *Dyes and Pigments*, 2019, 162, 232-242.

[40] J.W. Cai, P. Zhao, H.J. Niu, Y.F. Lian, C. Wang, X.D. Bai, W. Wang, Reducing polyazomethine to poly(*N*-phenylbenzylamine) with near infrared electrochromic, fluorescence and photovoltaic properties, *Polym. Chem.*, 2013, 4, 1183-92.

[41] X.C. Ma, H.J. Niu, H.L. Wen, S.H. Wang, Y.F. Lian, X.K. Jiang, C. Wang, X.D. Bai, W. Wang, Synthesis and electrochromic, halochromic and electrooptical properties of polyazomethines with a carbazole core and triarylamine units serving as functional groups, *J. Mater. Chem. C*, 2015, 3, 3482-93.

Table captions:

Table 1. Elemental analysis of the PAs.

Table 2. Inherent viscosities, GPC data and thermal properties of the PAs.

Table 3. Solubilities of the PAs.

Table 4. Electrochemical properties of the PAs.

Table 1. Elemental analysis of the PAs.

Polymer	Formula (molecular weight)	Elemental analysis (%)			
			C	H	N
PA-VIIIA	$(C_{56}H_{40}N_6O_4S)_n$ $(893.02)_n$	Calcd	75.3 %	4.5 %	9.4 %
		Found	75.2 %	4.4 %	9.7 %
PA-VIIIB	$(C_{56}H_{40}N_6O_3)_n$ $(844.95)_n$	Calcd	79.6 %	4.8 %	10.0 %
		Found	79.5 %	4.6 %	9.8 %
PA-VIIIC	$(C_{59}H_{40}F_6N_6O_2)_n$ $(978.98)_n$	Calcd	72.4 %	4.1 %	8.6 %
		Found	72.6 %	4.3 %	8.8 %
PA-VIIID	$(C_{50}H_{36}N_6O_2)_n$ $(752.86)_n$	Calcd	79.8 %	4.8 %	11.2 %
		Found	79.6 %	5.0 %	11.3 %

Table 2. Inherent viscosities, GPC data and thermal properties of the PAs.

Polymer	η (dL/ g) [a]	GPC data[b]			DSC	TGA		
		$M_w \times 10^4$	$M_n \times 10^4$	PDI	T_g [c] (°C)	$T_{5\%}$ [d] (°C)	$T_{10\%}$ [e] (°C)	Char yield [f] (%)
PA-VIIIA	0.50	3.8	2.1	1.8	320	340	448	62
PA-VIIIB	0.75	4.4	2.3	1.9	303	456	530	66
PA-VIIIC	0.62	5.2	2.6	2.0	301	390	520	69
PA-VIIID	0.70	3.6	2.1	1.7	315	448	531	65

[a] Determined with 0.5% solutions in a solvent (DMAc) at 25 °C.

[b] Relative to polystyrene standard, using DMF as the eluent.

[c] Baseline shift in the second heating DSC traces, with a heating rate of 20 °C/min in nitrogen.

[d, e] temper at 5% and 10% weight loss were recorded by TGA at a heating at 10 °C/min in nitrogen.

[f] Residual weight (%) when heated to 800 °C.

Table 3. Solubilities of the PAs.

Polymer	Solvents								
	NMP	DMAc	DMF	DMSO	THF	EtOH	$CHCl_3$	Actone	ethanol
PA-VIIIA	++	++	+	++	-	-	-	-	-
PA-VIIIB	+	+	+	+	-	-	-	-	-
PA-VIIIC	++	++	+	++	-	-	-	-	-
PA-VIIID	+	+	+	+	-	-	-	-	-

Note: 0.01 g sample is dissolved in 1mL of solvent.

"++" Soluble at room temperature.

"+" heated to dissolve.

"-" Insoluble even on heating.

Table 4. Electrochemical properties of the PAs.

Index	NMP solution λ/nm		Oxidation Potential[a](V)			E_g[b] (eV)	HOMO[c] (eV)	LUMO[d] (eV)
	Abs.$_{max}$	Abs.$_{onset}$	E_{onset}	$E_{ox1\ 1/2}$	$E_{ox2\ 1/2}$			
PA-VIIIA	330	339	0.50	0.97	1.69	3.12	4.82	1.70
PA-VIIIB	340	396	0.58	0.96	1.68	3.13	4.90	1.77
PA-VIIIC	341	406	0.31	0.67	1.57	3.05	4.63	1.58
PA-VIIID	339	417	0.30	0.63	1.58	2.97	4.62	1.65

[a] Oxidation half-wave potentials from cyclic voltammograms.

[b] The data were calculated by the equation: $E_g = 1240/\lambda_{onset}$ of polymer film.

[c] The HOMO energy levels were calculated from cyclic voltammetry and were referenced to ferrocene (4.8 eV).

[d] LUMO = HOMO - E_g.

Figure captions:

Scheme 1. Synthetic pathway toward the monomer.

Scheme 2. Synthetic pathway toward the polymers PA-VIII (A-D).

Figure 1. ^{1}H NMR spectrum of monomer V. This spectrum was recorded in DMSO-d_6.

Figure 2. COSY spectrum of monomer V. This spectrum was recorded in DMSO-d_6.

Figure 3. ^{13}C NMR spectrum of monomer V. This spectrum was recorded in DMSO-d_6.

Figure 4. ^{1}H NMR spectrum of monomer VI. This spectrum was recorded in DMSO-d_6.

Figure 5. COSY spectrum of monomer VI. This spectrum was recorded in DMSO-d_6.

Figure 6. ^{13}C NMR spectrum of monomer VI. This spectrum was recorded in DMSO-d_6.

Figure 7. FT-IR spectra of the PAs.

Figure 8. ^{1}H NMR spectrum of PA-VIIID. This spectrum was recorded in DMSO-d_6.

Figure 9. Tapping mode AFM topography image of the PA-VIIID film (4 µm × 4 µm).

Figure 10. UV-Vis spectra of the PA. These spectra were recorded in NMP.

Figure 11. Fluorescence spectra of the PAs. These spectra were ecorded in NMP.

Figure 12. TGA thermograms of the PAs.

Figure 13. Repeated CV of PA-VIIID and ferrocene on an ITO-coated glass substrate in a 0.1 M Bu_4NClO_4/CH_3CN solution.

Figure 14. Electrochemistry of the PA-VIIID thin films on ITO coated glass substrates at various applied potentials in a 0.1 M Bu_4NClO_4/CH_3CN solution.

Figure 15. CIE plot of the PA-VIIID film on an ITO-coated glass substrate at various applied potentials in a 0.1 M Bu_4NClO_4/CH_3CN solution.

Figure 16. Electrochemistry of thin PA-VIIID films on ITO-coated glass substrates at various applied potentials in a 1 M hydrochloric acid solution.

Figure 17. CIE plot of a PA-VIIID film on an ITO-coated glass substrate at various applied potentials in a 1 M hydrochloric acid solution.

Figure 18. Changes in the light transmission at 424 nm for a PA-VIIID film on an ITO-coated glass substrate and current density during a switching study in a 0.1 M Bu_4NClO_4/CH_3CN solution.

Figure 19. Changes in the light transmission at 820 nm for a PA-VIIID film on an ITO-coated glass substrate and current density during a switching study in a 0.1 M Bu_4NClO_4/CH_3CN solution.

Figure 20. Transmittance curve for PA-VIIID circulating at 424 nm in a 0.1 M Bu_4NClO_4/CH_3CN solution.

Figure 21. Transmittance change curve for PA-VIIID at 820 nm in a 0.1 M Bu_4NClO_4/CH_3CN solution.

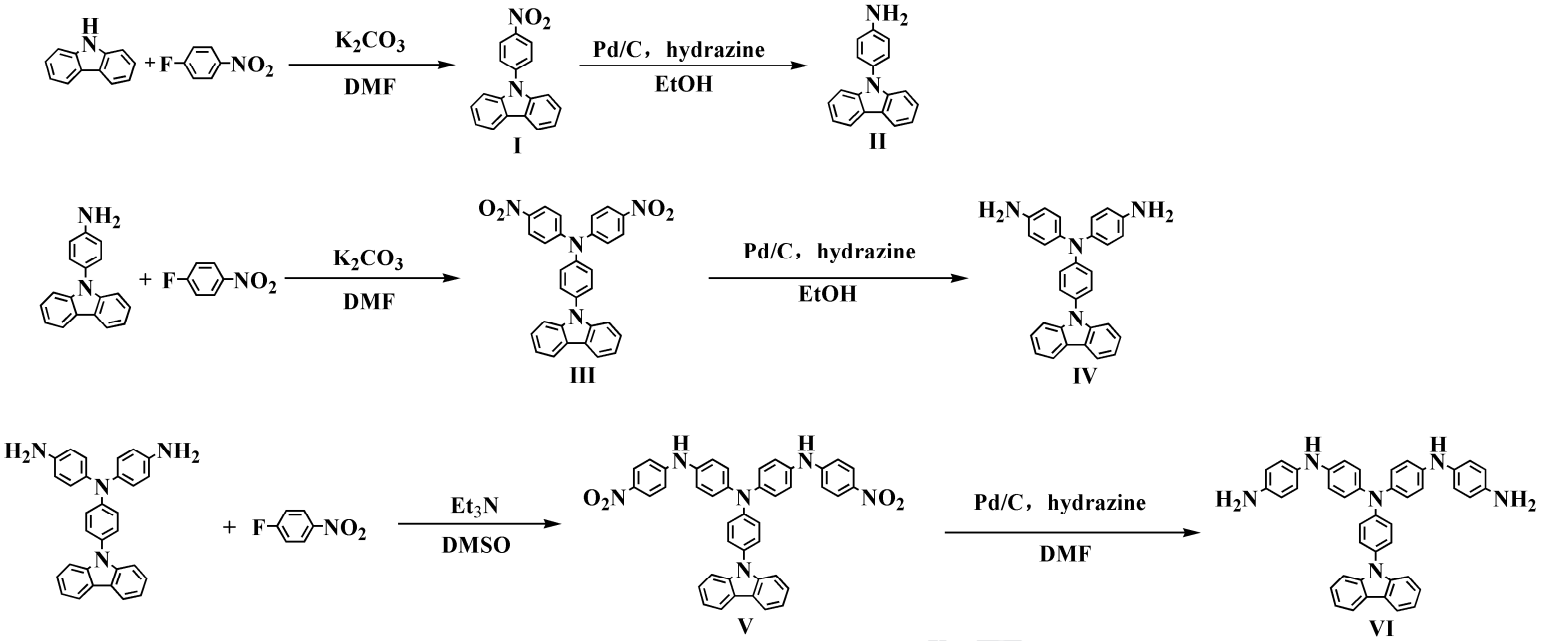

Scheme 1. Synthetic pathway toward the monomer.

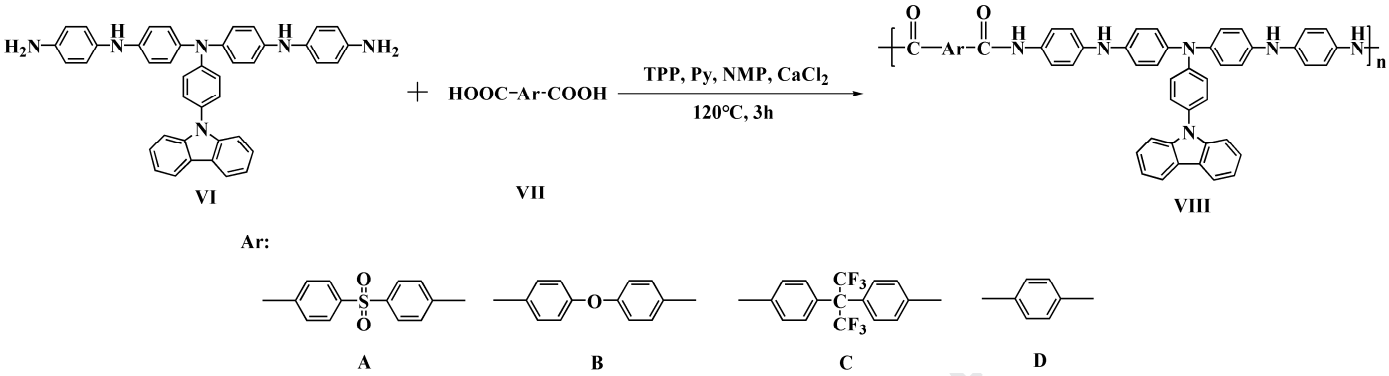

Scheme 2. Synthetic pathway toward the polymers PA-VIII (A-D).

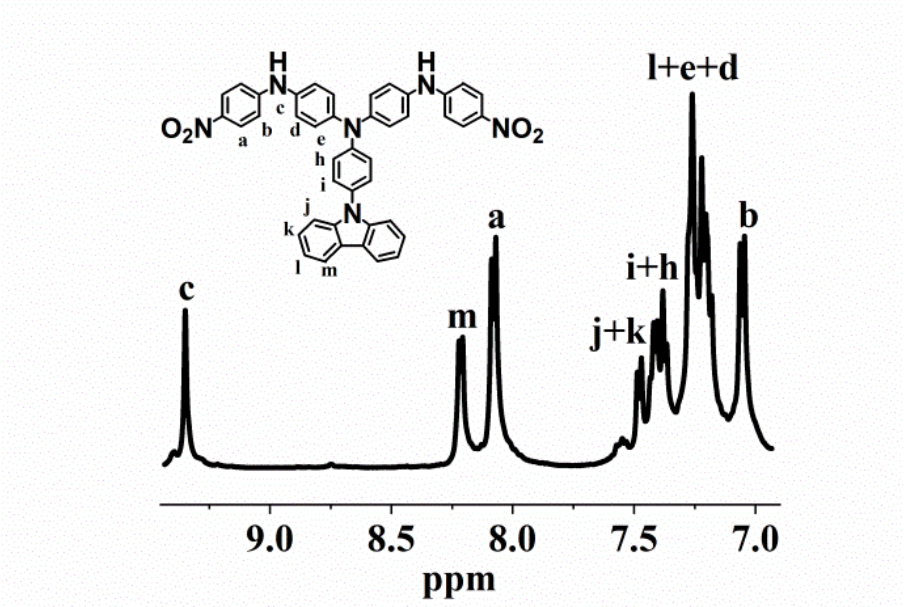

Figure 1. ^{1}H NMR spectrum of monomer V. This spectrum was recorded in DMSO-d_6.

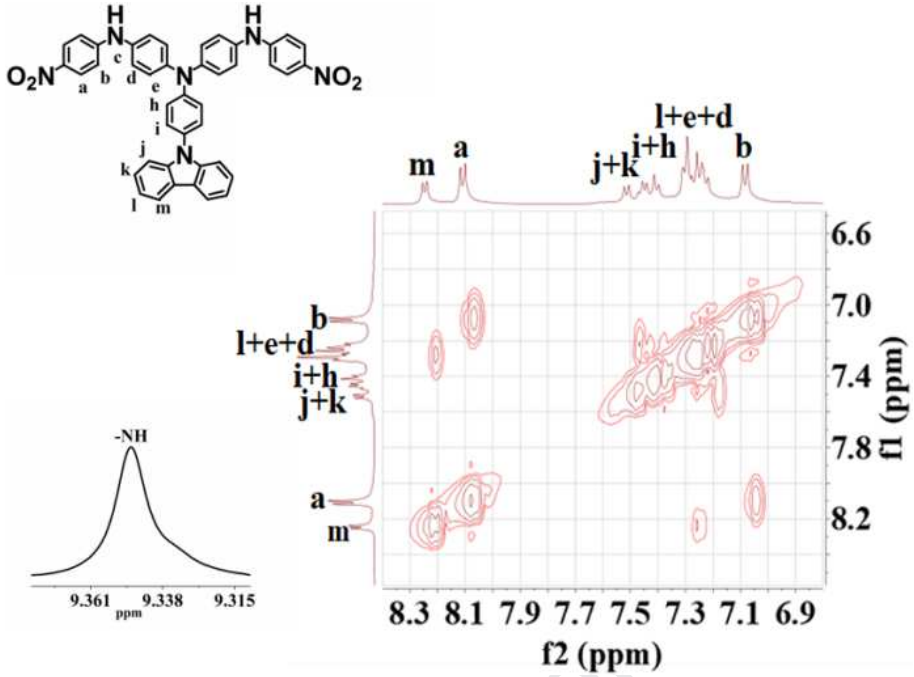

Figure 2. COSY spectrum of monomer V. This spectrum was recorded in DMSO-d_6.

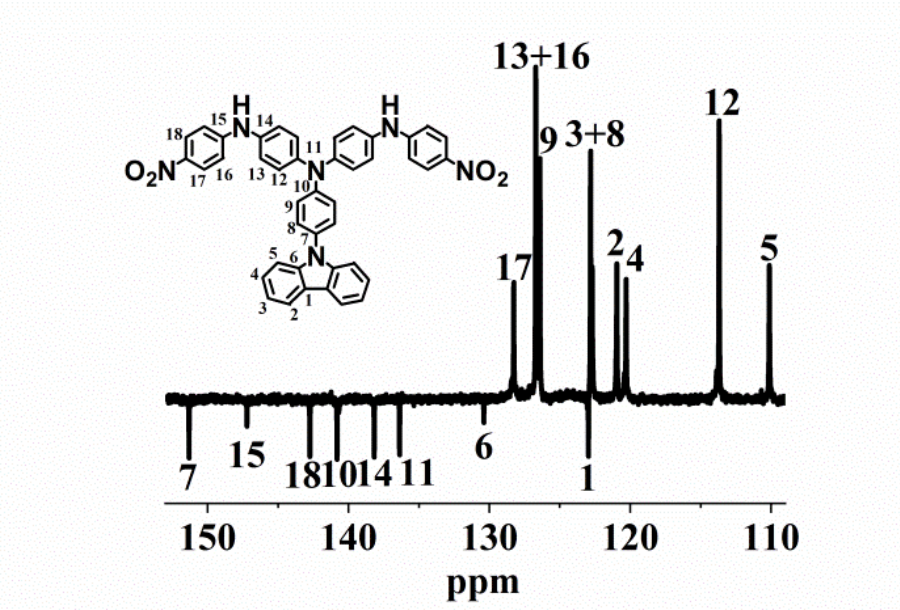

Figure 3. ^{13}C NMR spectrum of monomer V. This spectrum was recorded in DMSO-d_6.

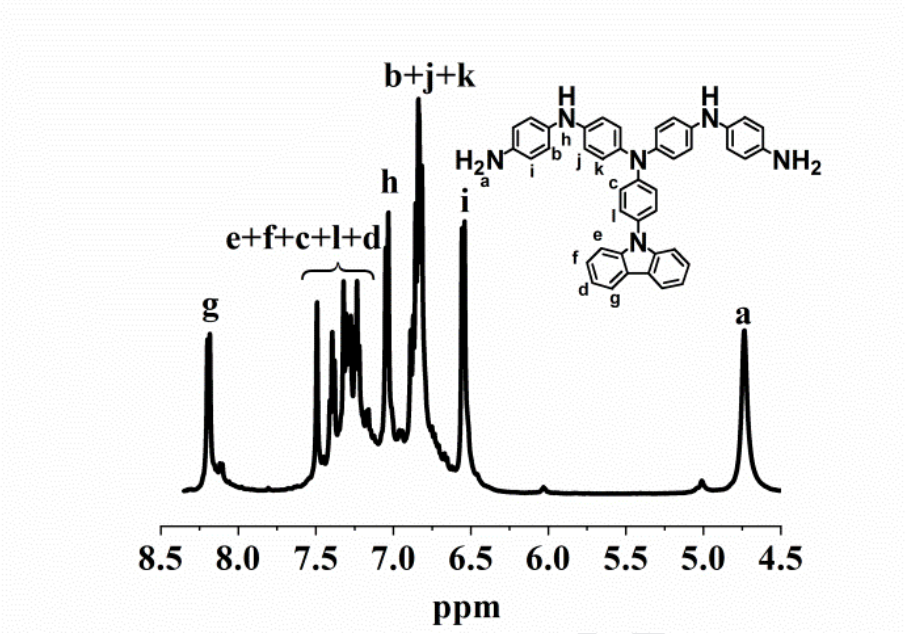

Figure 4. ^{1}H NMR spectrum of monomer VI. This spectrum was recorded in DMSO-d_6.

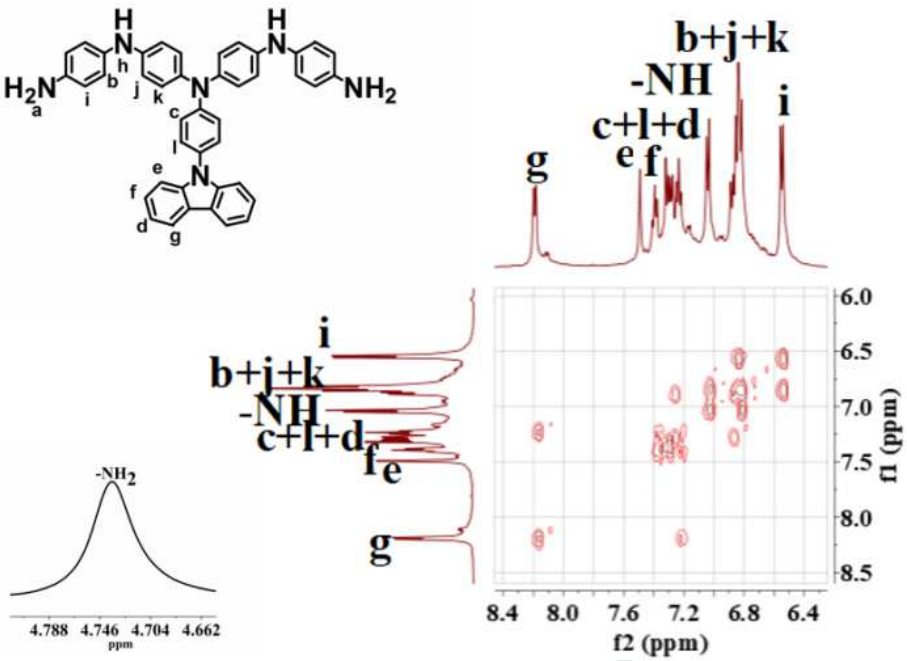

Figure 5. COSY spectrum of monomer VI. This spectrum was recorded in DMSO-d_6.

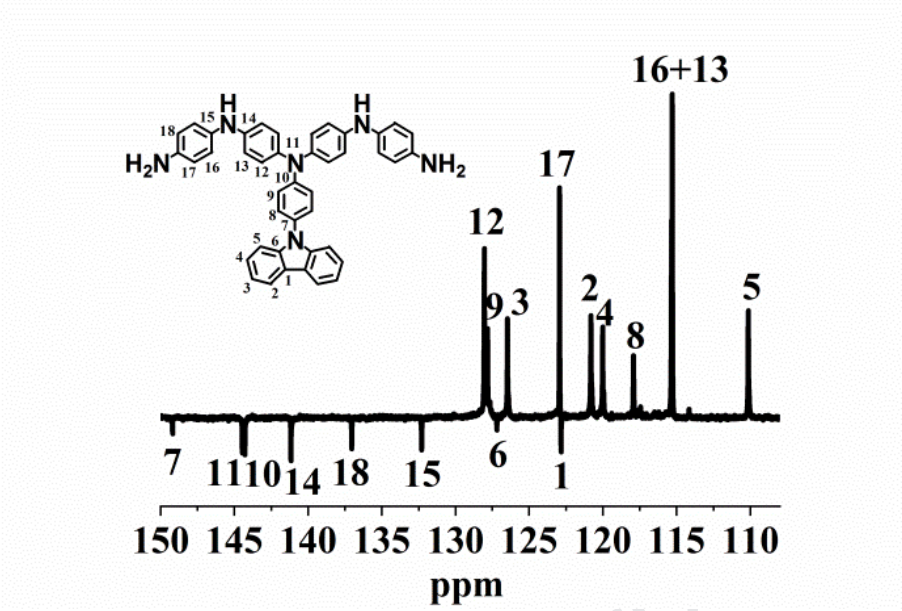

Figure 6. ^{13}C NMR spectrum of monomer VI. This spectrum was recorded in DMSO-d_6.

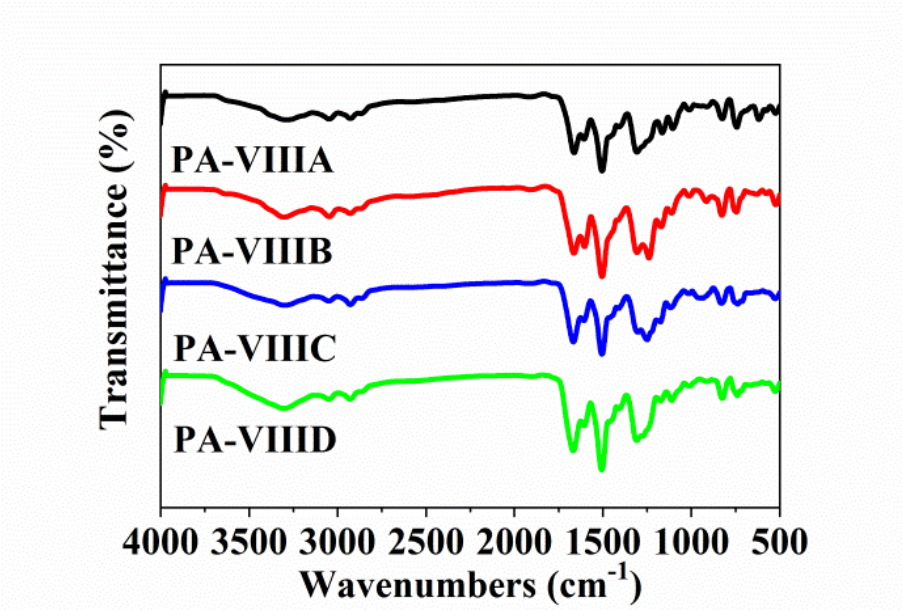

Figure 7. FT-IR spectra of the PAs.

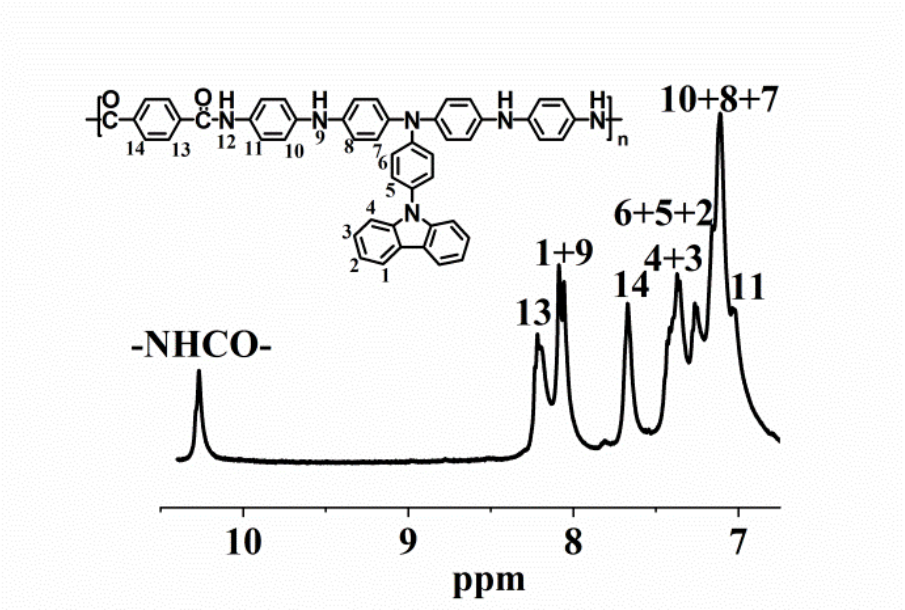

Figure 8. ^{1}H NMR spectrum of PA-VIIID. This spectrum was recorded in DMSO-d_6.

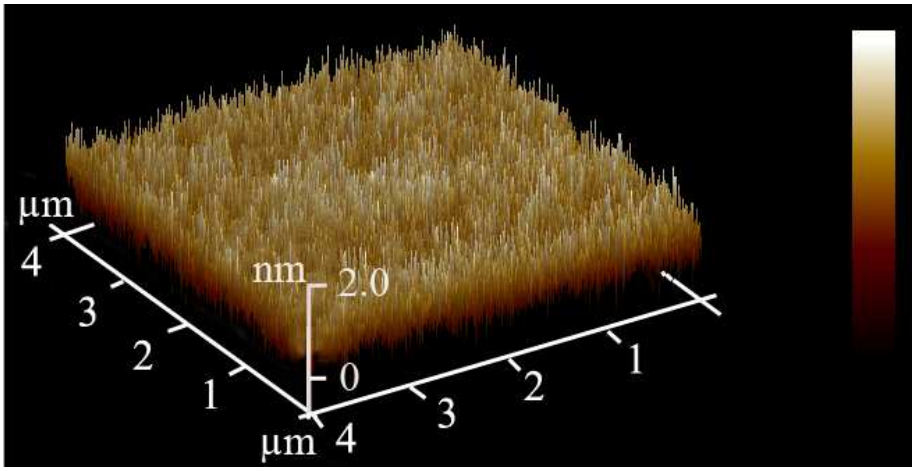

Figure 9. Tapping mode AFM topography image of the PA-VIIID film (4 µm × 4 µm).

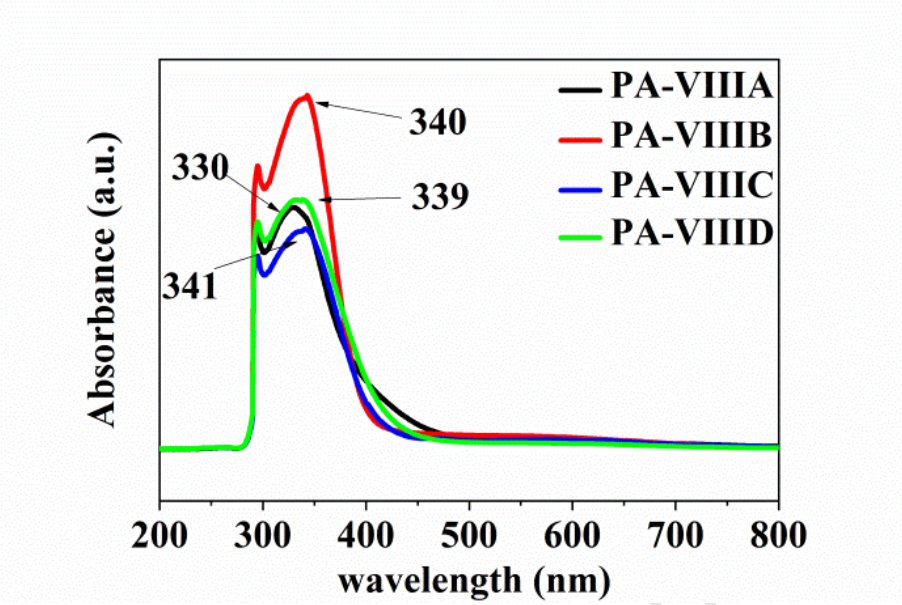

Figure 10. UV-Vis spectra of the PAs. These spectra were recorded in NMP.

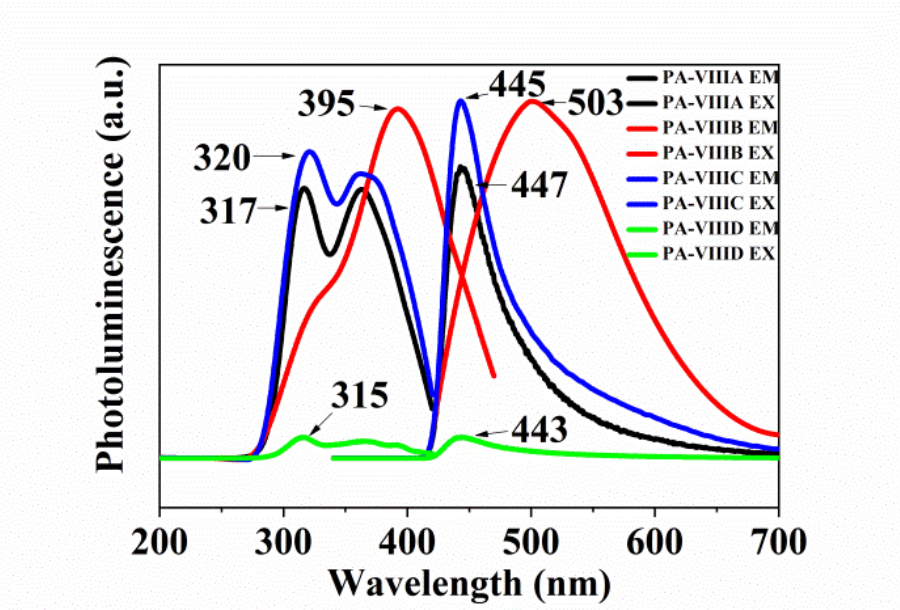

Figure 11. Fluorescence spectra of the PAs. These spectra were recorded in NMP.

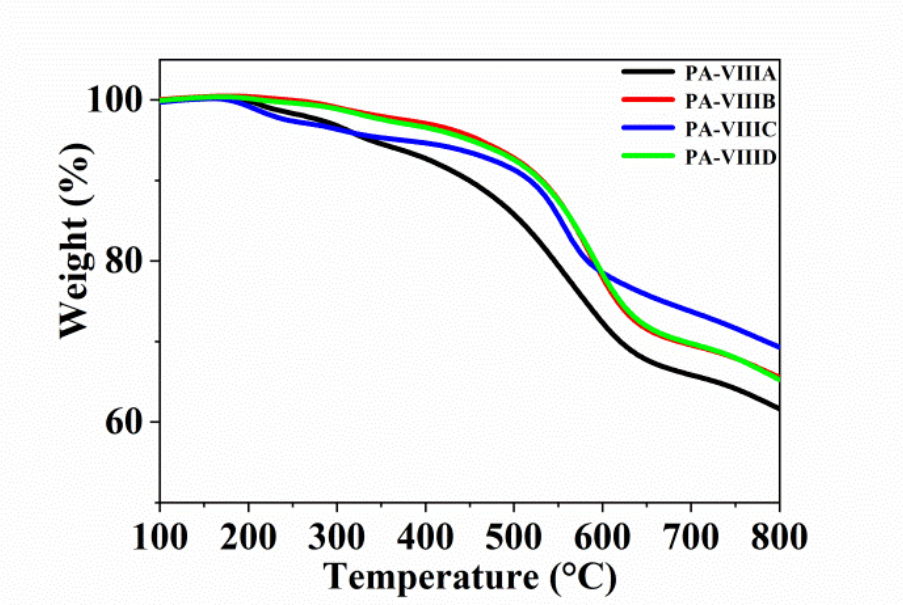

Figure 12. TGA thermograms of the PAs.

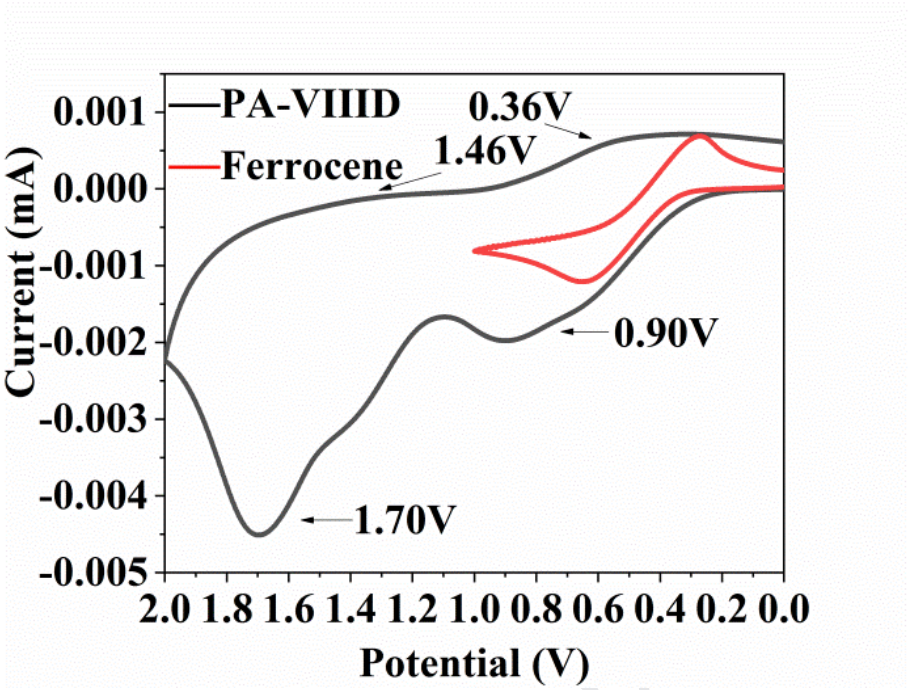

Figure 13. Repeated CV of PA-VIIID and ferrocene on an ITO-coated glass substrate in a 0.1 M Bu_4NClO_4/CH_3CN solution.

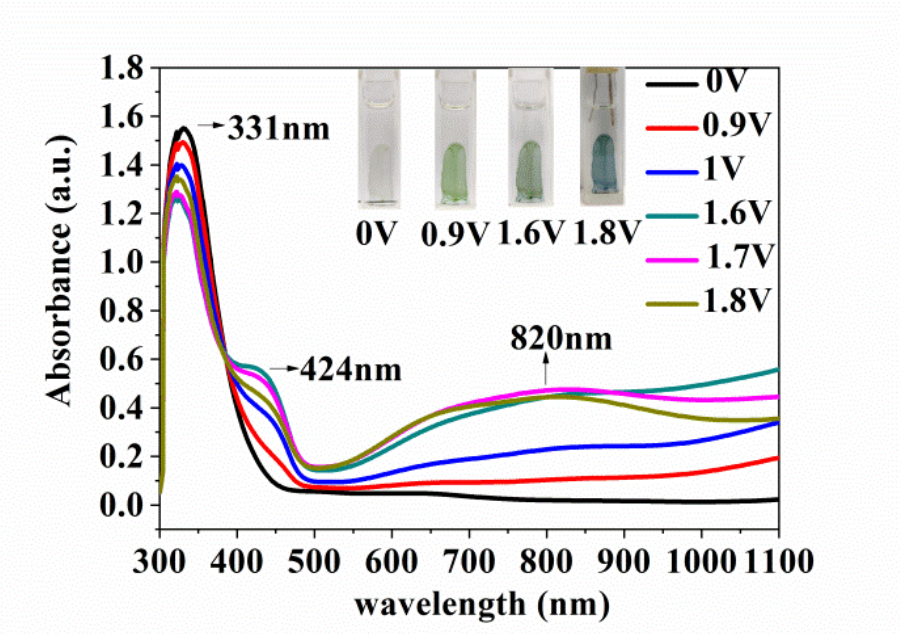

Figure 14. Electrochemistry of the PA-VIIID thin films on ITO-coated glass substrates at various applied potentials in a 0.1 M Bu_4NClO_4/CH_3CN solution.

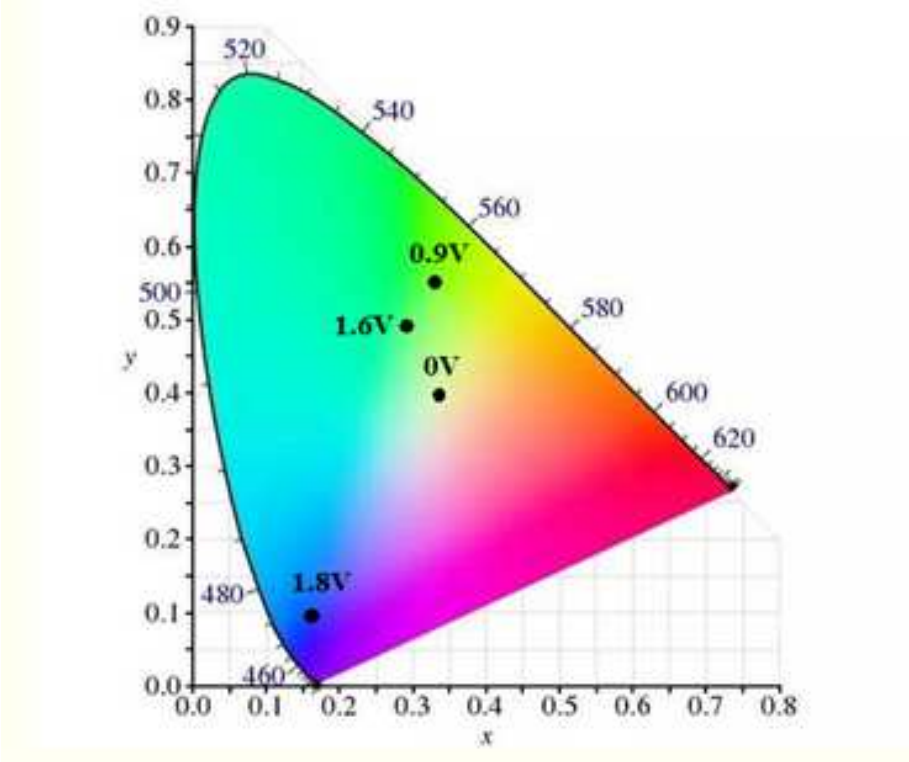

Figure 15. CIE plot of the PA-VIIID film on an ITO-coated glass substrate at various applied potentials in a 0.1 M Bu_4NClO_4/CH_3CN solution.

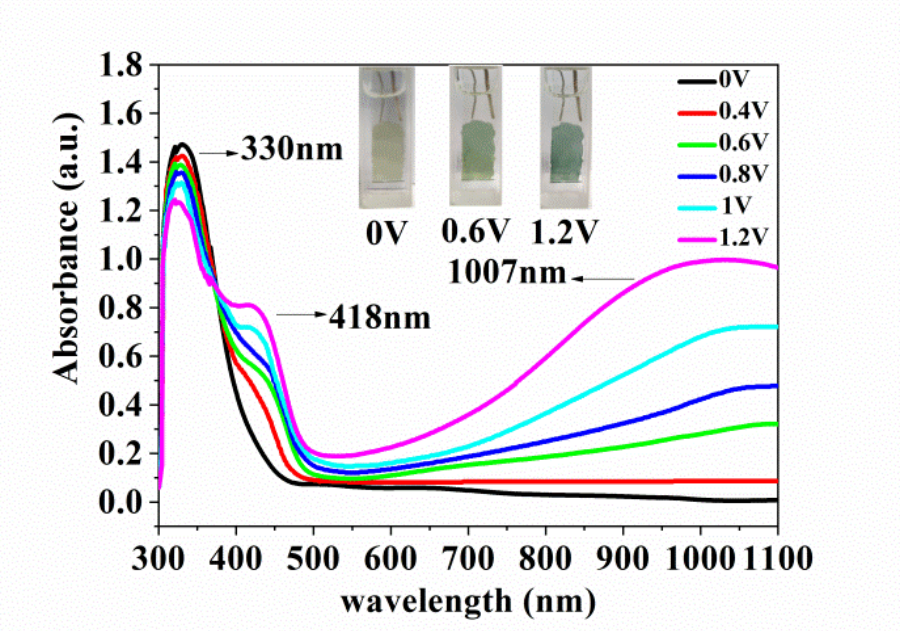

Figure 16. Electrochemistry of thin PA-VIIID films on ITO-coated glass substrates at various applied potentials in a 1 M hydrochloric acid solution.

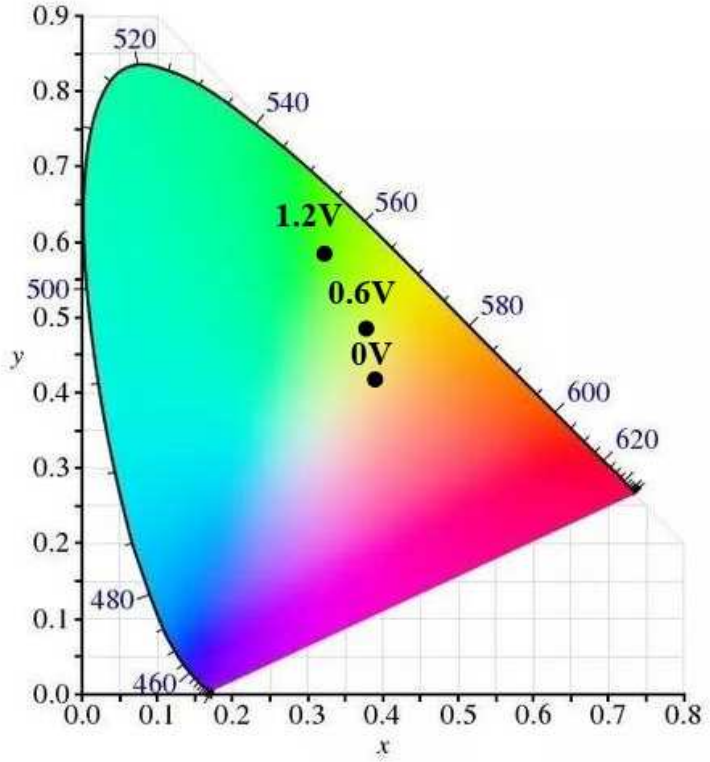

Figure 17. CIE plot of a PA-VIIID film on an ITO-coated glass substrate at various applied potentials in a 1 M hydrochloric acid solution.

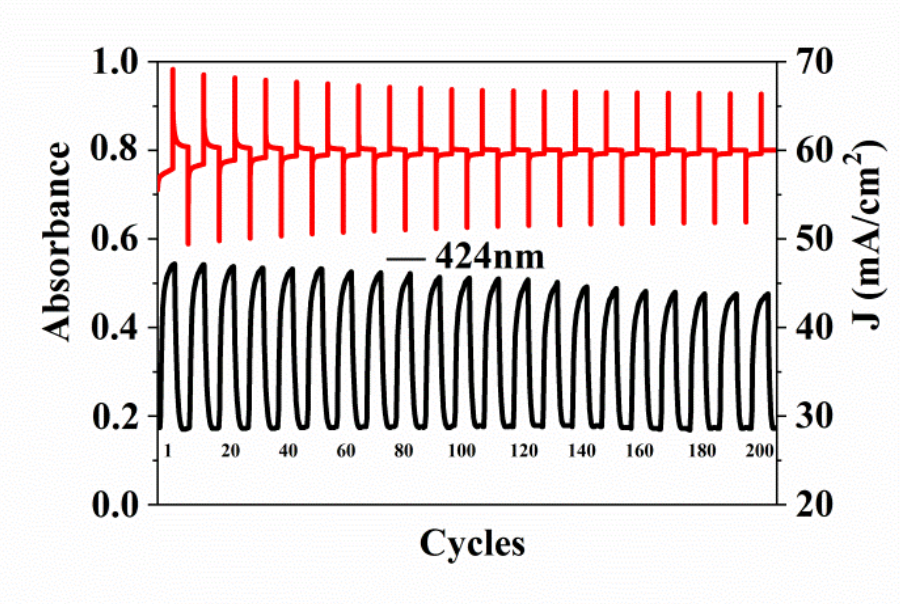

Figure 18. Changes in the light transmission at 424 nm for a PA-VIIID film on an ITO-coated glass substrate and current density during a switching study in a 0.1 M Bu_4NClO_4/CH_3CN solution.

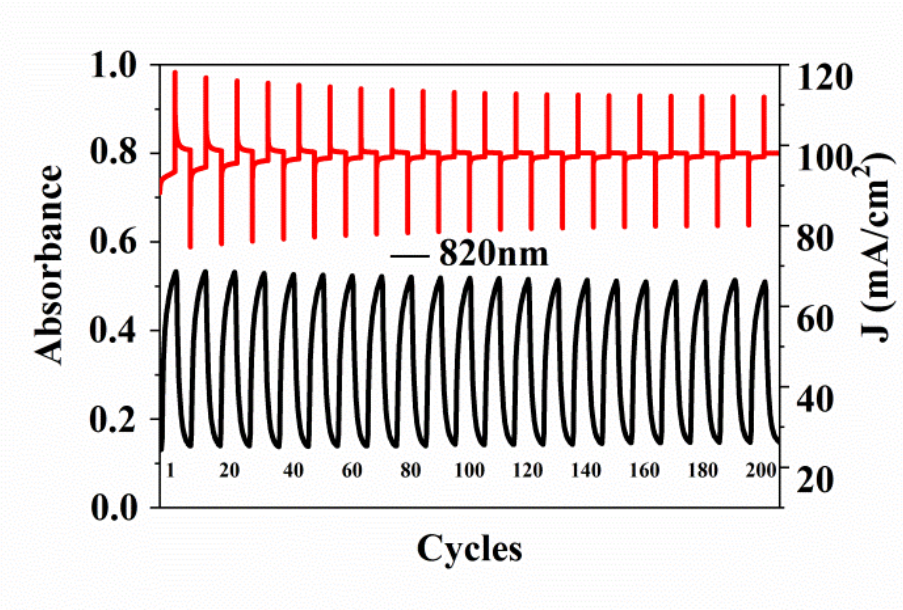

Figure 19. Changes in the light transmission at 820 nm for a PA-VIIID film on an ITO-coated glass substrate and current density during a switching study in a 0.1 M Bu_4NClO_4/CH_3CN solution.

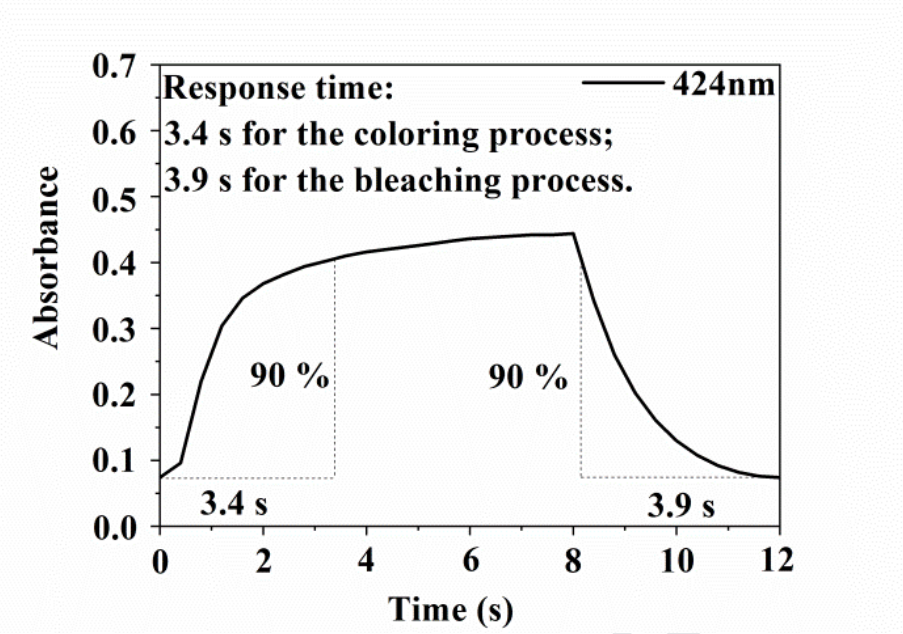

Figure 20. Transmittance curve for PA-VIIID circulating at 424 nm in a 0.1 M Bu_4NClO_4/CH_3CN solution.

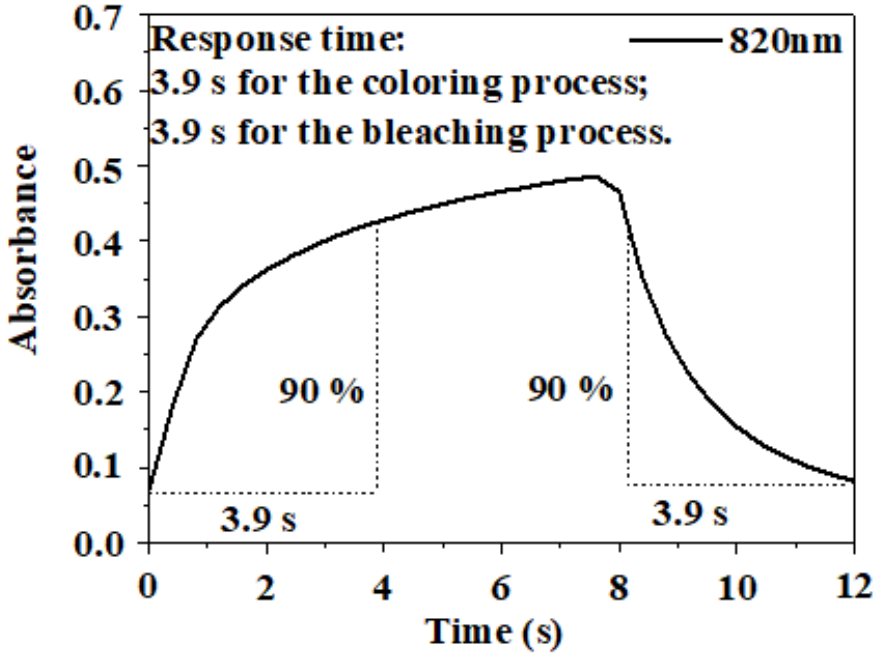

Figure 21. Transmittance change curve for PA-VIIID at 820 nm in a 0.1 M Bu_4NClO_4/CH_3CN solution.

Highlights

1. Successfully synthesized a series of novel redox active polyamides PA (VIIIA-VIIID) with three color-changing groups of aniline, triphenylamine and carbazole structures.

2. The polyamides were highly soluble in various solvents, had excellent thermostability, prolonged cycling stability, high color contrast, and rapid switching speeds.

3. The polyamides exhibit electrochromic properties in organic electrolyte solutions and hydrochloric acid.

Conflict of interest

To the best of our knowledge, the named authors have no conflict of interest, financial or otherwise.

All authors have declare that: no support, financial or otherwise, has been received from any organization that may have an interest in the submitted work ; and there are no other relationships or activities that could appear to have influenced the submitted work.